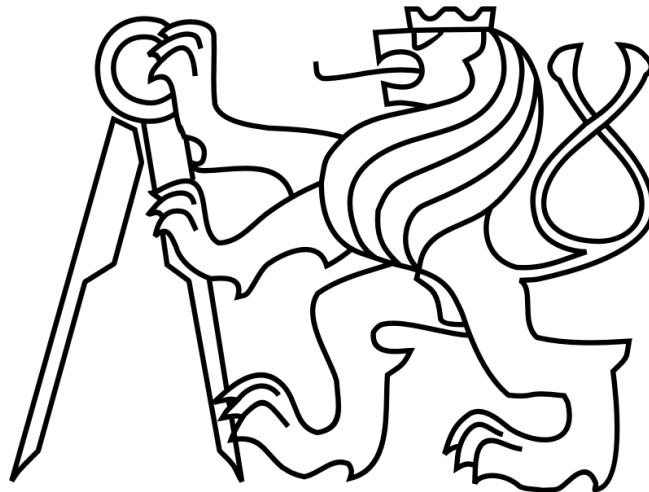


CZECH TECHNICAL UNIVERSITY IN PRAGUE

FACULTY OF MECHANICAL ENGINEERING

DEPARTMENT OF PROCESS ENGINEERING



FLOW PROPERTIES OF COLLAGEN MATTER

BACHELOR THESIS

Supervisor: doc. Ing. Jan Skočilas, Ph.D.

2020

Hadeel Atallah



BACHELOR'S THESIS ASSIGNMENT

I. Personal and study details

Student's name:	Atallah Hadeel	Personal ID number:	463673
Faculty / Institute:	Faculty of Mechanical Engineering		
Department / Institute:	Department of Process Engineering		
Study program:	Bachelor of Mechanical Engineering		
Branch of study:	Power and Process Technology		

II. Bachelor's thesis details

Bachelor's thesis title in English:
Flow properties of collagen matter

Bachelor's thesis title in Czech:
Flow properties of collagen matter

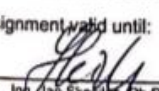

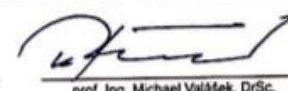
Guidelines:
The identification of flow properties of investigated material, especially when the material exhibits Non-Newtonian behavior, which is usual for food, is preceding key step in the design of the equipment determined for material transport, e.g. in pipes. The aim of the work is the assessment of the flow properties of the collagen matter in the capillary rheometer. The aims of the thesis are:
1) Perform literature search of collagen flow properties, flow in slit and capillary rheometer.
2) Acquaint with experimental equipment in the laboratory, method of measurement and data treatment methodology.
3) Assemble own approach in the form of a short program or script to evaluate experimental data.
4) Evaluate provided experimental data and obtain flow properties of collagen matter.

Bibliography / sources:
FRATZL, Peter. Collagen: structure and mechanics. New York: Springer, [2008]. ISBN 978-0-387-73906-9.
BARNES, Howard A., J. F. HUTTON a Kenneth WALTERS. An introduction to rheology. New York: Distributors for the U.S. and Canada, Elsevier Science Pub. Co., 1989. Rheology series, 3. ISBN 9780444871404.

Name and workplace of bachelor's thesis supervisor:
Ing. Jan Skočilas, Ph.D., Department of Process Engineering, FME

Name and workplace of second bachelor's thesis supervisor or consultant:

Date of bachelor's thesis assignment: **30.04.2020** Deadline for bachelor thesis submission: **07.08.2020**
Assignment valid until: **30.09.2020**

  
Ing. Jan Skočilas, Ph.D. prof. Ing. Tomáš Jirout, Ph.D. prof. Ing. Michael Valášek, DrSc.
Supervisor's signature Head of department's signature Dean's signature

III. Assignment receipt

The student acknowledges that the bachelor's thesis is an individual work. The student must produce her thesis without the assistance of others, with the exception of provided consultations. Within the bachelor's thesis, the author must state the names of consultants and include a list of references.

14/7/2020 hadeel
Date of assignment receipt Student's signature

Annotation List

Name: Hadeel

Surname: Atallah

Title Czech: Flow Properties of Collagen Matter

Title English: Flow Properties of Collagen Matter

Scope of work:

number of pages: 82

number of figures: 47

number of tables: 39

number of appendices: 5

Academic year: 2019-2020

Language: English

Department: Department of Process Engineering

Specialization: Power and Process Engineering

Supervisor: doc. Ing. Jan Skočilas, Ph.D

Reviewer:

Tutor:

Submitter:

Keywords: Collagen; Rheology; Flow properties; Power-law; Capillary Rheometer

Affidavit

I confirm that the bachelor's work was disposed by myself and independently, under the lead of my thesis supervisor. I stated all sources of the documents and literature.

In Prague

.....

Hadeel Atallah

Acknowledgements

I would like to express my gratitude towards my supervisor doc. Ing. Jan Skočilas, Ph.D for his expert guidance throughout this thesis. I would also like to thank Ing. Jaromír Štancl, Ph.D and Ing. Jan Stipek for their assistance during the experiments, and my family for their constant support.

Abstract

This thesis is aimed at the identification of flow parameters of the investigated collagen material. General information about collagen, general rheology and rheology of high viscous materials, and types of rheometers is presented. Essentially, the flow properties of bovine-extracted collagen solution with a dry-content of 9.69 % are investigated using a capillary rheometer equipped with three different slit dies manufactured at the Czech Technical University in Prague. The experimental data is processed using a MATLAB code where the power-law model is fitted to find the consistency coefficient and the power-law index of collagen matter.

Table of Contents

1	Introduction	8
2	Literature Review	9
2.1	Collagen	9
2.2	Model Fluids	13
2.3	Rheology	14
2.3.1	Flow and Deformation	15
2.3.2	Classification of Fluids	17
2.3.3	Newtonian Fluids	17
2.3.4	Non-Newtonian Fluids.....	19
2.3.5	Time-Independent Fluids	19
2.3.6	Time-Dependent Fluids	27
2.3.7	Viscoelastic Fluids and Effects of Viscoelasticity	28
2.4	Rheometry	33
2.4.1	Slit Rheometry	35
2.5	Summary of Literature Review	38
3	Experiments	40
3.1	Method of Measurement	43
3.2	Method of Data Processing	45
3.3	Results and Discussion.....	51
4	Conclusion	68
5	References	69
6	Appendices	72
	List of Symbols.....	72
	List of Tables	74
	List of Figures	76
	Appendix A: Procedure of Calculation of a Point in Rheogram	78

1 Introduction

The flow properties of materials are essential information for the design of transport devices. This thesis is focused on the investigation of flow properties of a specific kind of collagen matter. Collagen is a gel-like (for high water content) and a dough-like (for low water content), non-Newtonian, viscoelastic substance used in wide applications including the biomedical and industrial fields. Until recently, the studies done on this material dealt with solutions of low collagen concentrations. The aim of this work is the investigation of flow properties of collagen material required by engineers for designing transport equipment including pipes and pumps.

First, a literature search about collagen, including its hierarchical structure, types, uses, methods of extraction, and general properties is performed. In addition, three model fluids for testing devices for the measurement of flow properties will be also discussed. A review of rheology, the basics of flow and deformation and the classification of fluids, specifically, non-Newtonian behaviour with respect to collagen matter consistency follows.

Furthermore, the most common mathematical expressions used to model fluid behaviour will be explored. From rheometry, which deals with the methods of finding rheological properties of materials, a suitable rheometer and experimental method, with favourable measuring conditions mimicking typical industrial processes like the extrusion of sausage casings, will be chosen. The assessment of experimental data for finding the flow parameters of a collagen solution sample with a dry content of 9.69 % in the form of a rheogram will be done using MATLAB. Finally, a comparison between the findings of this and other researches is presented.

2 Literature Review

2.1 Collagen

Proteins are one of the most plentiful organic molecules involved in every aspect of cellular life. From catalytic enzymes that carry out thousands of chemical reactions in cells to structural components that eventually allow movement, proteins have the most diverse range of functions. A special type of proteins that offers numerous mechanical advantages is collagen [1].

Collagen is a hard, insoluble protein made of amino acids called glycine, proline, hydroxyproline and arginine. Collagen makes up approximately one-third of all proteins within the human body and other mammals [2]. Collagen is found in corneas, bones, blood vessels, cartilage, dentin of teeth, etc. In photosynthetic and unicellular organisms, polysaccharides and cellulose replace collagen's profuse role. As a fibrous structural protein, collagen is found in the extracellular matrix. The extracellular matrix (ECM) is a three-dimensional network of the non-cellular macromolecules present within all tissues and organs that provides not only scaffolding but also biochemical support for all surrounding cells [3, 4].

Currently, there are 29 different proteins identified as collagens in the human body [9]. Collagen nomenclature follows roman numerals. The most prevalent types of collagen are type I, II, III, IV, and V. Individual members of the collagen family belong to different classes of collagen [3]. The first class are the fibrillar collagens which constitute of the most widely occurring collagen type I. In addition to type I, types II, III, V, XI, XXIV and XXVII are also part of fibrillar collagens. The remaining collagen subfamilies are classified into fibril associated and related collagens, beaded filament forming collagen, basement membrane and associated collagens, short chain collagens and related proteins, transmembrane collagens and collagen-like proteins, collectins and ficolins, and other collagens and collagen-like proteins [5].

The common feature of all types of collagen is the right-handed triple helical structure. Three polypeptide chains of approximately 1000 amino acids are wound together forming a triple helix. These chains are referred to as α –chains. They consist of a repeated sequence of amino acids which in turn form collagen varying in size, function, and location. Each α –chain is an extended left-handed helix with a pitch of 18 amino acids per turn. Hydrogen bonds hold the three chains together. The most common type of collagen; type I,

consists of two chains called $\alpha 1$ and $\alpha 2$. Essential to the triple helical structure formation is the existence of glycine residue. Glycine is the smallest amino acid therefore filling up the restricted spaces of the chain and allowing tight packing around the central axis of the molecule. In this way, glycine occupies every third position of the polypeptide forming a sequence -Gly-X-Y- where the X position is frequently proline and the Y position is hydroxyproline.

The total length of the triple helical domain is about 300 nm. The triple helical structure described is typical for fibrillar collagens. For other collagen types, polypeptide chains are much shorter or contain sections of non-helical domains. Finally, collagen supra-molecules form fibrils which in turn form collagen fibres. Figure 1 outlines collagen structure [6, 7].

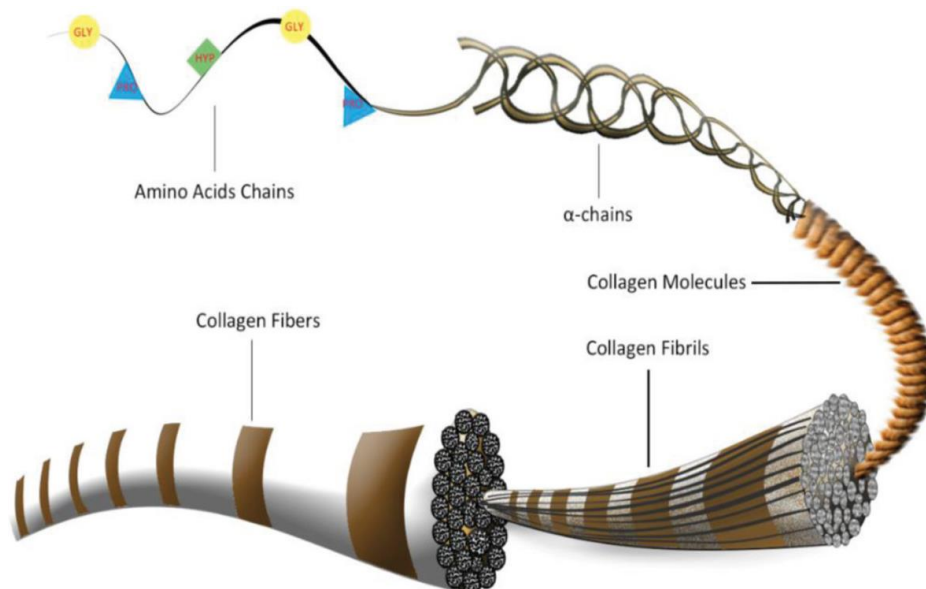


Figure 1: Structure of fibrillar collagen [7]

Inadequacy of industrial collagen is impossible since collagen is the most abundantly available protein in all mammals and some marine organisms. Collagen can be extracted from bovine, porcine, and fishes. Other sources include chicken, kangaroo tail, rat tail tendon, duck feet, horse tendon, alligators' bone and skin, birds' feet, ovine source like sheep skin, and frog skin [3]. Collagen extraction methods and processing after extraction greatly affect its characteristics; therefore, for each industrial application, a purpose-specific

procedure as well as raw material is used. Beginning from the raw materials, by-products of animal slaughter are the main source of industrial collagen. Before collagen is extracted, it must go through a pre-treatment process. In this process, non-collagenous substances and proteins are removed. As a result of collagen's complex structure previously described, its dissolution is a slow process even in boiling water. Therefore, pre-treatment involves chemicals that break its cross-links before extraction. The chemicals used are either diluted acids or bases. Then, partial hydrolysis, a process in which chemical bonds are broken with water, is used to break collagen's cross-links however keeping the collagen chains unbroken. In the case of an acidic pre-treatment, the raw material is placed in an acidic solution at a controlled temperature. This in turn causes the raw material to swell from 2 to 3 times its initial volume splitting the non-covalent bonds (cross-links).

On the other hand, an alkaline pre-treatment is done with a basic solution of sodium chloride, sodium hydroxide, or calcium hydroxide (most commonly, sodium hydroxide). Pre-treatment with a basic solution can last from a few days up to several weeks. For fragile raw materials like porcine and fish, an acidic pre-treatment is optimum. However, for bovine, which is characterised as a thicker material, a more destructive chemical agent is used for full penetration into the raw material [3, 8].

After pre-treatment, chemical hydrolysis and enzymatic hydrolysis are employed as extraction means to obtain the final product. In chemical hydrolysis, organic acids such as acetic acid, citric acid and lactic acid, and inorganic acids such as hydrochloric acid are used. More commonly, due to the favourable efficiency, organic acids are often used. Specifically, acetic acid resulting in higher solubility of collagen. Finally, after extraction, a filtration process used for the separation of residue from the collagen solution is employed. In contrast, enzymatic hydrolysis extraction process makes use of enzymes that act as catalysts for chemical reactions. In this process, the raw material is added to acetic acid containing a specific enzyme such as pepsin then subjected to filtration. In enzymatic hydrolysis, the raw material could also be residue from chemical hydrolysis.

The choice of hydrolysis depends on the industrial requirements of the final product. For example, enzymatic hydrolysis produces less waste, has less processing time but is more expensive than chemical hydrolysis. In addition, enzymatic hydrolysis is preferred for products with a requirement of high nutritional value. Nevertheless, chemical hydrolysis is more common in industrial processes [8].

The complexity and rigidity of collagen's structure results in overall high mechanical strength. Collagen's mechanical strength varies depending on its biological role and is majorly affected by the length and diameter of collagen fibres, the type of collagen present and the distribution of collagen fibres. Just as crystalline polymers, which are polymers arranged into orderly crystalline structures, collagen's tensile deformation mechanism can be divided to four regions. The first region is known as toe or low strain region. In this region, macroscopic crimps are gradually removed from a collagen fibril. This allows for an undamaging longitudinal deformation of the fibril. After approximately 2 % strain to the collagen fibril, the second region known as the heel region starts. In this stage, collagen crimps are straightened, and the fibrils are further elongated. Next, the collagen fibril enters the elastic region. In this case, all the crimps in a collagen fibril are elongated and no further straightening is possible. Finally, collagen undergoes defibrillation under large stresses. In this process, multiple microfibrils break down dismantling the collagen network [9].

Another property of proteins known as denaturation outlines their structure and consequently their function because of increasing temperature and/or the addition of an acid or base. It is important to mention that the denaturation temperature of the collagen protein is greatly affected by collagen calcification- the mineralization of collagen by a calcium compound [10].

The non-calcified collagen in bone has a denaturation temperature of 60 °C. On the other hand, calcified collagen has a denaturation temperature 90 °C greater than non-calcified collagen [11]. However, according to a study by the Journal of Orthopaedic Research on The Role of Collagen in Determining Bone Mechanical Properties, calcified-collagen denaturation commences at approximately 120 °C and is completed at 190 °C. As a result of these differences, the study suggests that varying mineralization of collagen in bone could be the culprit of these inconsistencies [10, 11].

2.2 Model Fluids

When a new measurement device is developed e.g. for rheological measurements, its methodology must be validated by some well known ‘model’ fluids. The most common materials exhibiting viscoelastic behaviour (such as collagen) are carboxymethyl cellulose (CMC), polyamic acid (PAA), and M1 fluid.

Carboxymethyl cellulose is a nontoxic water-soluble cellulose derivative [26]. CMC has numerous industrial applications including its use in the food industry to increase viscosity of sauces and syrups and increase the richness of beverages. It is also used in the soaps, detergents, textile industry as a coating, paper industry and has been recently found to have health benefits when consumed. A study on the rheological properties of CMC showed that it exhibits, for highly concentrated solutions, a strong thixotropic behaviour [27, 28]. A comprehensive study of CMC is out of the scope of this thesis and further reading can be found in references [27, 28, 29].

On the other hand, Polyamic Acid (PAA) solutions are a precursor of polyimides [30]. Polyimides are engineering polymers with unique properties like the ability to withstand temperatures above 500 °C, chemical resistance and mechanical toughness [31]. PAA solutions exhibit viscoelastic fluid behaviour and are used in microelectronic devices. Experiments on the rheological properties, viscoelastic behaviour, as well as the applications of PAA can be found in references [30, 31, 32, 33].

The final fluid, known as M1, is a constant viscosity elastic liquid [34]. It was first developed at the Monash University as a ‘model’ fluid to unify rheological experiments and study the behaviour of viscoelastic fluids. In any case, neither the author nor the supervisor of this thesis was able to find information regarding the composition of the M1 fluid. Further reading on M1 and its rheological classification can be found in references [34, 35, 36, 37].

2.3 Rheology

Rheology is the field of science concerned with the flow and deformation of all matter [12]. The field of ‘Rheology’ was formally acknowledged in 1929 by a special organization known as The Society of Rheology [13]. Prior to that, widespread interest, and centuries worth of ongoing rheological research among scientists had been taking place. For instance, in 1678, Robert Hooke proposed his linear law for solid substances describing the dependency between stress and strain. Later, Isaac Newton introduced the concept of what is now known as viscosity in his hypothesis: “the resistance which arises from the lack of slipperiness of the parts of the liquid, other things being equal, is proportional to the velocity with which parts of the liquid are separated from one another” [14]. However, these descriptions account only for the two extreme ends in rheology: Hookean solids and Newtonian Fluids.

The first account of deviation from classical extremities was seen in experiments done by Wilhelm Weber. Weber’s experiments on silk threads resulted in a behaviour that is now identified as that of a viscoelastic solid. In these experiments, a tensile force was applied to a silk fibre. At first, the response was like that of metals; immediate elastic extension followed by slow and continuous extension with time. Then, as the load was removed another immediate extension occurred. However, Weber found that the silk fibre finally returned its original dimensions [14].

On the other hand, British scientist James Clerk Maxwell’s research contributed to fluid-like materials. These fluids are referred to by rheologists as viscoelastic liquids; materials that satisfied Maxwell’s equation relating stress, strain, and viscosity. Finally, by the beginning of the 20th century, it was clear that the rheology describing all materials was confined neither to Hookean solids nor to Newtonian fluids [14]. Today, rheological importance is evident in numerous industrial sectors. Personal care products, pharmaceutical and food industries, as well as the manufacturing industry utilize rheological data to perfect their products [15].

In the following review of rheology, the basics of flow and deformation are discussed first. Next, the classification of fluids as well as the different types of flows are explained. Furthermore, distinct ways of graphical representations of rheological data as well as theories and equations of several models describing fluid flow are shown. Finally, viscoelasticity and rheometry are discussed.

2.3.1 Flow and Deformation

Since rheology is the science primarily concerned with the flow and deformation of all matter, it is important to define the parameters essential to understanding the behaviour of matter when acted upon by forces. Depending on the motion of adjacent particles in a fluid, the two basic types of flows are extensional and shear flows. Shear flow is characterised by the *shear* motion of particles over or past one another. On the other hand, extensional flow is the motion of particles away from or towards one another [12].

A formal mathematical description of shear viscosity follows directly from the explanation of shear flow. Therefore, there exists a hypothetical model depicting shear flow as layers of the fluid sliding over each other. In this idealization, the bottom-most layer is stationary, and the velocity increases linearly with respect to each individual fluid layer [12, 15]. Figure 2 shows a fluid's hypothetical layers in shear flow.

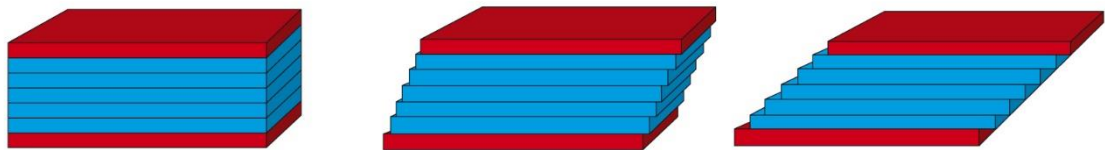


Figure 2: Individual layers of fluids in shear flow [15]

Shear stress is defined as the shear force per shear area. Shear stress is applied in the direction parallel to the face of a material. When shear stress is applied, the uppermost layer moves with a certain velocity. From this, we can introduce shear rate as the velocity gradient perpendicular to the flow; velocity divided by the shear gap. Shear rate is also referred to as strain rate, deformation rate and shear gradient [12, 15]. Shear stress and shear rate are related by a coefficient of proportionality known as viscosity or shear viscosity described by Newton's Law.

Viscosity is a property quantifying a fluid's resistance to flow [17]. All fluid flow, whether gases or liquids, exhibit viscous effects to some extent. It is important to mention that the equations (1), (2), and (3) are for simple shear flow and accurate rheological measurements should be done in laminar or homogeneous flow in which fluid layers exhibit

little or no mixing. Another type of viscosity is kinematic viscosity; shear viscosity divided by the fluid's density [15, 16].

Equations (1), (2), (3), and (4) describe shear stress, shear rate, shear viscosity and kinematic viscosity, respectively.

$$\tau = \frac{F}{A} \quad (1)$$

where:

τ [Pa] is shear stress

F [N] is shear force

A [m²] is shear area

$$\dot{\gamma} = \frac{V}{h} \quad (2)$$

where:

$\dot{\gamma}$ [s⁻¹] is shear rate at shear flow

V [m/s] is velocity

h [m] is shear gap

$$\eta = \frac{\tau}{\dot{\gamma}} \quad (3)$$

where:

η [Pa. s] is shear viscosity

τ [Pa] is shear stress

$\dot{\gamma}$ [s⁻¹] is shear rate

$$\nu = \frac{\eta}{\rho} \quad (4)$$

where:

ν [m²/s] is kinematic viscosity

η [Pa. s] is shear viscosity

ρ [kg/m³] is density

2.3.2 Classification of Fluids

The previous section was a brief introduction to rheological parameters and basic equations. In this and following sections, a division between fluid types depending on their behaviour is presented. Fluids are divided into two major groups: real fluids and ideal fluids. The latter is a group used as a simplification in fluid flow analysis. The difference between ideal and real fluids is in their compressibility and viscosity. All fluids fall into the *real fluids*' category which can be further sub-divided into the following types:

- Newtonian Fluids
- Non-Newtonian Fluids

2.3.3 Newtonian Fluids

Newtonian fluids are a class of fluids with a viscosity that remains constant with varying shear rate and shear stress at a constant temperature and pressure. Hence, for a Newtonian fluid, the shear rate and shear stress are directly proportional and therefore Newton's Law of viscosity shown in equation (3) is valid.

In Newtonian fluids, also called ideally viscous fluids, plotting shear stress vs. shear rate (flow curve) results in a straight line passing through the origin with a slope related to the shear viscosity. A common unit used for viscosity is poise. Poise is equivalent to 0.1 Pa·s [17]. Some examples of Newtonian fluids include water, mineral oil, salad oil, acetone as well as viscosity standards [15]. Figure 3 shows typical Newtonian fluids. The viscosity values are given in centipoise. Evidently, steeper slopes characterize higher viscosity values.

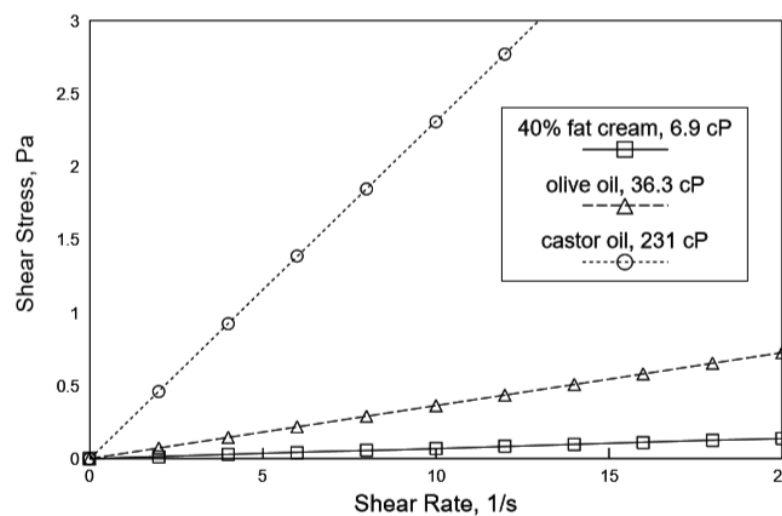


Figure 3: Rheogram of typical Newtonian fluids [16]

Although the viscosity of Newtonian fluids is constant, a dependency exists in certain variations in temperature and/or pressure. Generally, as the temperature increases, the viscosity of liquids decreases whereas the viscosity of gases increases [17]. In liquids, the rate of decrease in viscosity increases with higher viscosities. On the other hand, apart from extremely high pressures, liquids are independent of small pressure variations. For gases, kinematic viscosity is affected by pressure variations since their density is proportional to pressure. Therefore, as the pressure increases, a gas's kinematic viscosity varies [12, 17].

Furthermore, there is a limit to which fluids exhibit Newtonian behaviour. At extremely high shear rates, all liquids become Non-Newtonian [12]. At *critical* shear rates of approximately 10^5 s^{-1} , glycerol and mineral oils become Non-Newtonian. Figure 4 shows viscosity curves of silicone oils normally used as a Newtonian standard switching to Non-Newtonian behaviour at different shear rates and at a shear stress of 2000 Pa. The silicon oil with lowest critical shear rate has the highest molecular weight and hence the highest viscosity [12].

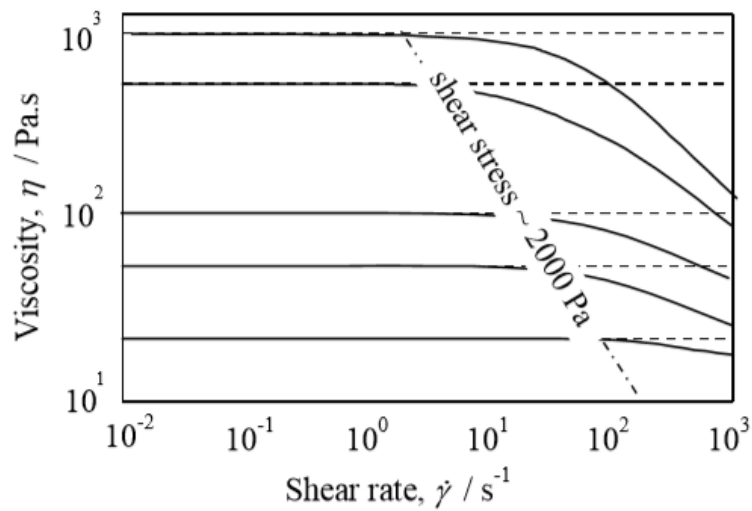


Figure 4: Viscosity curves for Silicon oils of different molecular weight [12]

2.3.4 Non-Newtonian Fluids

Non-Newtonian fluids are a class of substances comprising of all the fluids which do not follow Newton's law of viscosity, meaning their viscosity is dependent on the applied shear rate or shear stress, sometimes even on the kinematic history of the fluid [18]. Examples of non-Newtonian fluids include adhesives, biological fluids, pharmaceutical products as well as paints, polishes, and varnishes [18]. In a rheogram of shear stress vs. shear rate, this is seen as a curved line, a line that does not pass through the origin or both. Recall that for Newtonian substances, the constant of proportionality between stress and strain is shear viscosity that remains constant given constant pressure and temperature conditions. Contrarily, for a non-Newtonian fluid, the slope of its flow curve is referred to as apparent viscosity.

Therefore, when stating the *apparent* viscosity of a non-Newtonian substance it is important to mention the shear conditions; for example, $\eta(\dot{\gamma}) = 0.5 \text{ Pa}\cdot\text{s at } 10 \text{ s}^{-1}$ [15]. Non-Newtonian materials are grouped into three generalized classes as shown below [18]. These classes are further divided and will be discussed in the following.

- Time-independent fluids
- Time-dependent fluids
- Viscoelastic fluids

2.3.5 Time-Independent Fluids

As the name suggests, time-independent fluids are a class of non-Newtonian substances whose viscosity, given a constant temperature under shear, is not affected by time. The behaviour of time-independent fluids can be described by equation (5) and its inverse; this simply means that the value of the shear rate $\dot{\gamma}$ is directly determined by the instantaneous value of shear stress τ at that point and vice versa.

$$\dot{\gamma} = f(\tau) \quad (5)$$

Time-independent fluids, also referred to as 'purely viscous', 'inelastic', and 'generalized Newtonian fluids (GNF)', are further divided into the three following subgroups depending on the form of the function in equation (5) [18]. Below, further discussion of each subgroup of time-independent fluids follows.

- Shear thinning or pseudoplastic fluids
- Shear thickening or dilatant fluids
- Viscoplastic fluids

a) Shear Thinning/Pseudoplastic Fluids

The behaviour of shear thinning fluids is outlined by the decrease of their apparent viscosity with increasing shear rates. This is the most common type of non-Newtonian fluid behaviour. Examples of shear-thinning fluids include coatings, glues, shampoos, polymer solutions and polymer melts [15]. Evidently, the flow curves of shear-thinning fluids illustrated in figure 5 show that upon increasing shear rates, the viscosity of pseudoplastic fluids decreases [19].

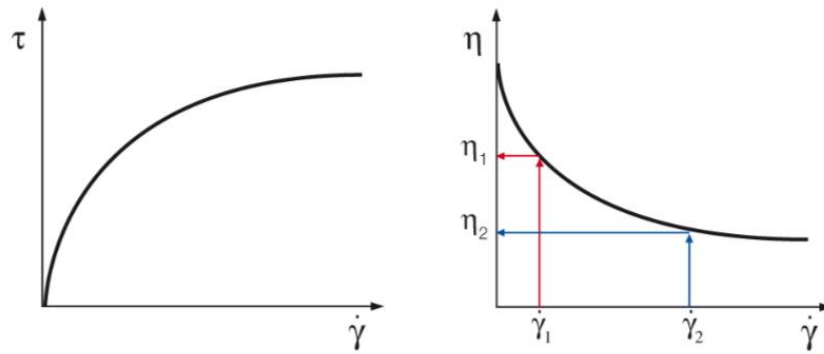


Figure 5: Flow curves of a shear-thinning fluid [15]

In the case of polymer solutions and melts, very low and very high shear rates result in Newtonian behaviour; flow curves are straight lines which pass through the origin in a linear scale. When using log-log viscosity plots at low enough shear rates, generally in the shear range below 1 s^{-1} , the resulting value of viscosity is constant and is known as the plateau value of the zero-shear viscosity η_0 . Similarly, at high shear rates, typically in the shear range above 1000 s^{-1} , another plateau value known as the infinite shear viscosity or limiting high-shear viscosity η_∞ is seen [15, 18].

Several mathematical expressions have been suggested to provide an empirical relation for shear stress and shear rate curves. The most preferred two-parameter model is known as the power-law or Ostwald-de Waele model. For shear-thinning fluids, the existence of a linear portion on the log-log scale flow curves indicates that the power-law model is applicable. Equation (6) shows the power-law:

$$\tau = K(\dot{\gamma})^n \quad (6)$$

where:

τ [Pa] is shear stress

K [Pa.s^{*n*}] is consistency coefficient

$\dot{\gamma}$ [s⁻¹] is shear rate

n [-] is flow behaviour index or power-law index

The power-law is generally sufficient to describe many non-Newtonian fluids with the exceptional disadvantage of very low shear rates. In addition, the power-law does not provide information regarding the values of zero-shear viscosity and infinite shear viscosity. In equation (6), the flow behaviour index ranges between 0 and 1 for shear-thinning fluids. Evidently, the lower the value of n , the higher the degree of shear-thinning. When $n = 1$, fluids are Newtonian in behaviour and when $n > 1$, the fluid is shear-thickening which will be discussed in the following. Figure 6 shows some materials' typical values of consistency and flow behaviour indices using the power-law model.

System	Temperature (K)	n (-)	K (Pa.s ^{<i>n</i>})
Agro- and food-related products			
Aerated poultry waste slurry (x is % volume of solids)	283–298	$1.81 - 0.161 \ln x$	$1.12 \times 10^{-11} (x)^{2.59}$
Ammonium alginate solution (3.37%)	297	0.5	13
Apple butter	–	0.15	200
Apple sauce	300	0.3–0.45	12–22
Apricot puree	300	0.3–0.4	5–20
Banana puree	293–315	0.33–0.5	4–10
Carrot puree	298	0.25	25
Chicken (minced)	296	0.10	900
Chocolate	303	0.5	0.7
Guava puree	296.5	0.5	40
Human blood	300	0.9	0.004

Figure 6: Typical values of power-law constants [18]

Another model proposed by Malcolm Cross (1965) is known as the Cross model or the Cross-viscosity equation. The Cross model is a four-parameter equation used to describe the behaviour of several fluids. This model gives Newtonian regions at both low and high shear rates therefore describing the entire flow curve of a shear-thinning fluid. The Cross-model is shown in equation (7).

$$\frac{\eta - \eta_{\infty}}{\eta_0 - \eta_{\infty}} = \frac{1}{1 + (K\dot{\gamma})^m} \quad (7)$$

In the equation (7), η_0 and η_{∞} are the plateau values of the apparent viscosity, while K and m are fitting parameters. It should be noted that K is not the consistency coefficient previously described in the power-law. In this case, the dimensions of K are that of time, while m is dimensionless. When using equation (7) to describe non-Newtonian fluids, the value of m determines the degree of shear-thinning. This means that when m tends to zero, the fluid exhibits Newtonian behaviour, as opposed to the most shear thinning liquids which have a value m tending to 1. Evidently, the Cross equation can be reduced to power-law, Newtonian, and Sisko models. Another model like Cross is known as the Ellis fluid model or the Meter model. Furthermore, for certain distinct values of the exponent, the Ellis model has been given other names; Williamson, Dougherty, Krieger, and Phillippoff Models. These models are out of the scope of this thesis and will not be used to fit the collagen flow curves. Another model like Cross is known as the Carreau viscosity equation or the Carreau model; both models are the same at very low and very high shear rates [12, 18].

At high shear rates, zero-shear viscosity becomes much greater than the limiting high-shear viscosity $\eta_0 \gg \eta_{\infty}$ and $K\dot{\gamma} \gg 1$ therefore simplifying equation (7) to the Sisko equation shown in equation (8).

$$\eta = \eta_{\infty} + \frac{\eta_0}{(K\dot{\gamma})^m} \quad (8)$$

Since the value of the exponent m is equal to one for most shear-thinning liquids, multiplying equation (8) by the shear rate gives another expression known as the Bingham equation, shown in equations (9) and (10). Viscoplastic behaviour and the Bingham plastic model will be further discussed in the following section [12, 15, 18].

$$\tau = \frac{\eta_0}{K} + \eta_{\infty}\dot{\gamma} \quad (9)$$

Or

$$\tau = \sigma_B + \eta_B\dot{\gamma} \quad (10)$$

where:

σ_B [Pa] is Bingham yield stress

η_B [Pa. s] is Bingham plastic viscosity

b) Shear Thickening/Dilatant Fluids

As their name suggests, shear thickening or dilatant fluids behave conversely to shear thinning fluids. When under shear, the apparent viscosity of dilatant fluids increases. This phenomenon was first observed in concentrated suspensions and only happens under very specific circumstances. The behaviour of shear thickening fluids is not yet clearly understood, and a possible explanation is that under high enough shear-rates, after the flow field organizes a fluid's particles into layers, particle ordering breaks down and the particles form clumps [12].

Furthermore, in some cases when high enough shear-rates are achieved, shear-blocking occurs. Shear-blocking is a phenomenon that occur when the apparent viscosity becomes so high that the flow completely comes to a stop. Typical examples of fluids exhibiting shear-thickening behaviour include concentrated suspensions of china clay, titanium oxide, and cornflour in water. It should be noted that the term dilatant is less favoured than shear thickening since not all shear thickening fluids 'dilate' or increase in volume upon shearing. The difficult nature of shear thickening fluids can be challenging in some technical processes like the blocking of nozzles in spraying and the damage of shafts in stirring processes [12, 15, 18, 19].

Like shear thinning behaviour, shear thickening fluids can be modelled using the power law model. Evidently from equation (6), when $n > 1$, the fluid exhibits shear thickening behaviour. Interestingly, some concentrated suspensions show both pseudoplastic and dilatant behaviour. At lower shear rates, using the power law model, $n < 1$. However, at high shear rates, $n > 1$, and shear thickening is observed. Figure 7 shows a log-log scale plot of shear thinning and shear thickening fluids modelled using the power law. Newtonian behaviour is also shown for comparison [18, 19].

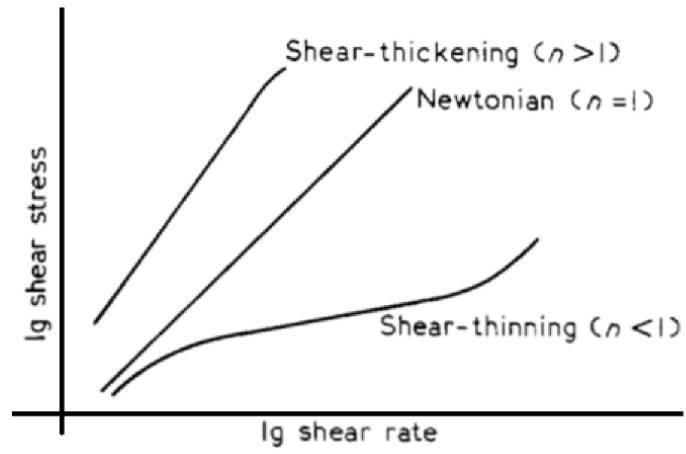


Figure 7: Log-log plot of shear stress vs. shear rate of shear thickening and shear thinning fluids [19]

c) Viscoplastic Fluids

Viscoplastic fluids are a class of non-Newtonian, time-independent fluids with a yield point. This means that these fluids have a yield stress that must be exceeded to flow. On the other hand, when the minimum yield stress is not achieved, such materials deform elastically. An example of this is the minimum force required for toothpaste to flow out of its tube. Consequently, the flow curves of such fluids will never pass through the origin and may be linear or non-linear. In case of a linear flow-curve, the fluid is known as a Bingham plastic and can be modelled using equation (10) where the slope of the shear stress-shear rate curve is Bingham's plastic viscosity η_B . However, when a substance's flow curve is non-linear with a yield stress, it is known as a yield-pseudoplastic material [12, 15, 18, 20].

In addition to the most common Bingham plastic model, viscoplastic behaviour can be modelled using the Herschel-Bulkley and Casson fluid models, sometimes also referred to as 'generalized Bingham model'. The Casson fluid model is often considered a better curve fitting tool than the Bingham plastic model since it considers the bend of the curve at lower shear rates. Equation (11) shows the two-parameter Casson model which is often used for food products like chocolate [12, 15, 18, 21].

$$\sqrt{\tau} = \sqrt{\sigma_C} + \sqrt{\eta_C \dot{\gamma}} \quad (11)$$

where:

σ_C [Pa] is Casson yield stress

η_C [Pa. s] is Casson plastic viscosity

τ [Pa] is shear stress

$\dot{\gamma}$ [s^{-1}] is shear rate

As previously stated, some substances' flow curves are non-linear after the yield point. Consequently, characteristics like shear thinning, shear thickening or even time-dependency is possible. In this case, the Herschel-Bulkley three-parameter model, shown in equation (12) is used to describe flow curves [15, 19]. Shown in equation (12), the parameter p describes the flow behaviour. If $p > 1$, the behaviour is shear thickening after the yield-point. If $p < 1$, the behaviour is shear thinning. Finally, if $p = 1$, the material exhibits Bingham flow behaviour [15].

$$\tau = \sigma_{HB} + c(\dot{\gamma})^p \quad (12)$$

where:

σ_{HB} [Pa] is Herschel-Bulkley yield stress

c [Pa. s] is flow coefficient; also called Herschel-Bulkley viscosity

τ [Pa] is shear stress

$\dot{\gamma}$ [s^{-1}] is shear rate

p [-] is Herschel-Bulkley index

Figure 8 shows, on a linear scale, the flow curves of all the previously discussed time-independent fluids. For comparison, Newtonian flow is also included.

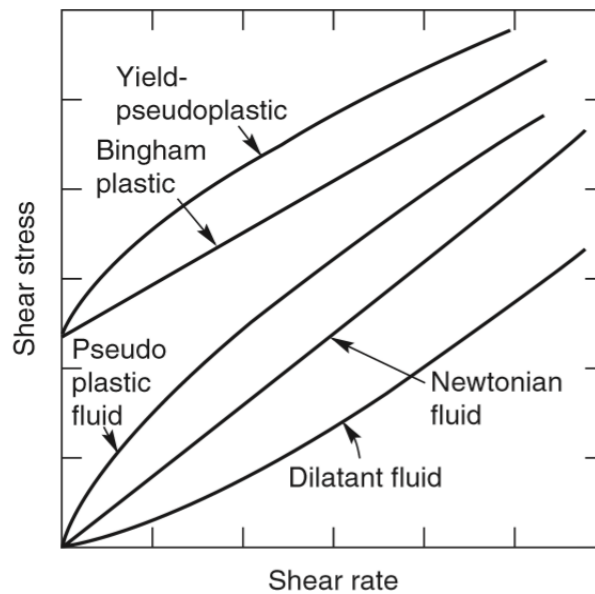


Figure 8: Flow curves of time-independent fluids [18]

2.3.6 Time-Dependent Fluids

Another class of non-Newtonian behaviour is known as time-dependent flow behaviour. As opposed to time-independent flow, time-dependent flow behaviour is characterized by the change of viscosity with the duration of shearing. Time-dependency can be further subdivided into the two following groups:

- Thixotropy
- Rheopexy or negative thixotropy

Thixotropic behaviour is the decrease of the apparent viscosity of a substance at a constant shear rate with time. In addition, in some cases, thixotropic substances regain their original rheological state in a time-dependent manner upon the removal of shearing. Examples of materials exhibiting such behaviour include cement pastes, protein solutions and foodstuff [15, 18].

On the other hand, in a case of the rare rheopectic behaviour, the apparent viscosity of a substance increases with time at a constant shear rate. Like thixotropic substances, rheopectic materials also regain their original rheological parameters upon the removal of shearing [15]. Figure 9 highlights the difference between time-dependent and time-independent fluids. In addition, the difference in behaviour of thixotropic and rheopectic materials is seen.

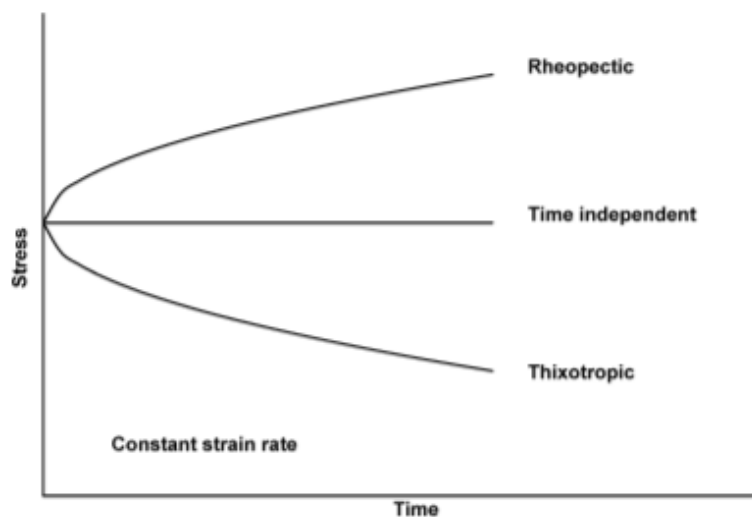


Figure 9: Time-dependent vs. time-independent flow behaviour [22]

2.3.7 Viscoelastic Fluids and Effects of Viscoelasticity

As their name suggests, viscoelastic fluids are materials that exhibit both viscous and elastic behaviour when sheared. Examples of such materials include hair shampoo, hand cream, polymer melts and synovial fluid [18]. Viscoelastic behaviour is limited on both ends by ideally elastic deformation and perfectly viscous flow. In the case of an ideal solid, when deformed elastically, the solid regains its original shape after the stress has been removed. When the applied stress exceeds a solid's yield stress, the original shape is not completely regained and the solid is said to flow, or more appropriately, creep. On the other hand, as previously stated, the shear stress is proportional to the shear rate in a perfectly viscous fluid (Newtonian fluid).

Viscoelasticity is a time-dependent response in which some material may recover instantly, others may recover with time while some may not recover at all after a load is removed [20]. There are two fields of viscoelasticity known as linear and non-linear viscoelasticity. In the linear viscoelastic field, viscoelastic materials are studied under low strain and deformation. However, in the non-linear viscoelastic field, materials are studied under large deformations [22]. Non-linear viscoelasticity is out of the scope of this thesis and will not be further discussed.

Given the complexity of viscoelastic behaviour, mathematical models and equations, and their corresponding mechanical analogies have been formulated by scientists to describe the combinational behaviour of the viscosity of fluids and the elasticity of solids [22]. These models use mechanical elements such as springs and dashpots [12]. The spring is considered an ideal element obeying Hooke's Law or the Law of Elasticity is shown in equation (13) below. On the other hand, the dashpot represents a viscous element obeying Newton's law presented in equation (3).

$$\tau = G\gamma \quad (13)$$

where:

τ [Pa] is shear stress

G [Pa] is shear modulus

γ [-] is shear strain

Maxwell's Model was the first known attempt to describe viscoelastic behaviour. This model, shown in figure 10, is made up of a spring and a dashpot connected in series. It is the simplest description of a viscoelastic liquid like hair shampoo [12].

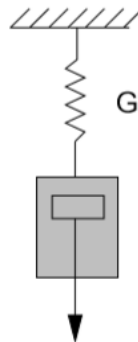


Figure 10: Scheme of the Maxwell model [16]

On the other hand, a spring and a dashpot connected in parallel represent the so-called Kelvin model or the Voigt-Kelvin model. The Voigt-Kelvin model, shown in figure 11, is the simplest description of a viscoelastic solid like hand cream [12].

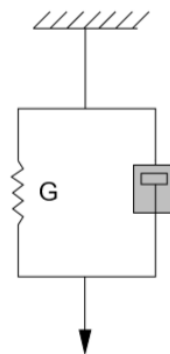


Figure 11: Scheme of the Kelvin-Voigt model [16]

Both models can be expanded, and a certain combination of springs and dashpots is not necessarily unique since several combinations can be used to model the same set of experimental data [12, 16]. When combining both the Maxwell model with the Kelvin-Voigt model in series, a third, more complicated model known as the Burgers model or the four-elements model arises.

It should be noted that, for a specific material, the use of any model requires a certain number and arrangement of springs and dashpots [12, 23]. Figure 12 shows the scheme of Burgers's model:

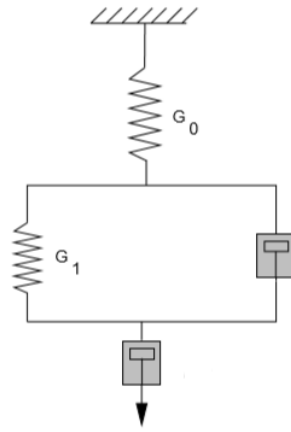


Figure 12: Scheme of the Burgers model [16]

- Effects of Viscoelasticity

Several unusual phenomena seen in the behaviour of many substances are directly linked to and caused by viscoelasticity. These effects may impose challenges in several processing industries like in the plastic, food, and printing sectors.

In printing processes, for example, some inks exhibit the clear viscoelastic effect of stringiness and tack. This is a mere ‘finger test’ for testing viscoelastic effects [15].

A more important viscoelastic effect is known as the Weissenberg or the rod-climbing effect as opposed to the inertial-dripping seen during the mixing of Newtonian fluids. The Weissenberg effect is evident, for example, during the mixing of cake batter.

In the process of designing extruders for shaping numerous food products, a viscoelastic effect commonly known as die swell or extrudate swell is often challenging. This phenomenon occurs when a viscoelastic material flows out of a capillary, tube, pipe, or bottle [15].

The Kaye effect, first observed by Arthur Kaye in 1963, is an effect that can be seen when pouring shampoo. This effect results in a sudden expulsion of a secondary jet of shampoo with a diameter larger than the primary one. Subsequently, the secondary jet collapses once it hits the primary jet. This occurrence has a duration of less than one second and has been under-researched by scientists, therefore lacking a proper explanation [24]. Figure 13 shows the series of events in the Kaye effect captured from a high-speed recording.

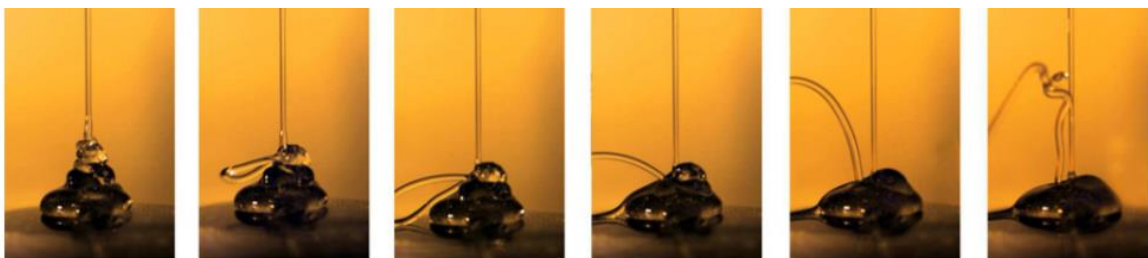


Figure 13: The Kaye effect captured in a series of images [24]

Other interesting viscoelastic effects include the tubeless siphon effect, which may happen in highly elastic fluids, the orange-peel or shark skin effect which may happen in blow moulding of hollow bodies like plastic bottles [16]. For visualization, figure 14 illustrates the previously mentioned effects of viscoelasticity in comparison with Newtonian fluids:

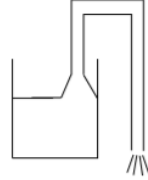
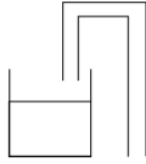
VISCOUS FLUID



VISCOELASTIC FLUID



WEISSENBERG
EFFECT



TUBELESS
SIPHON



JET SWELL

Figure 14: Effects of viscoelasticity in viscous versus viscoelastic fluids [16]

2.4 Rheometry

Rheometry refers to the experimental methods used by rheologists for determining rheological data. Likewise, a rheometer is a device used for measuring rheological properties. Rheometers can be divided into two basic groups shown in figure 15 [16].

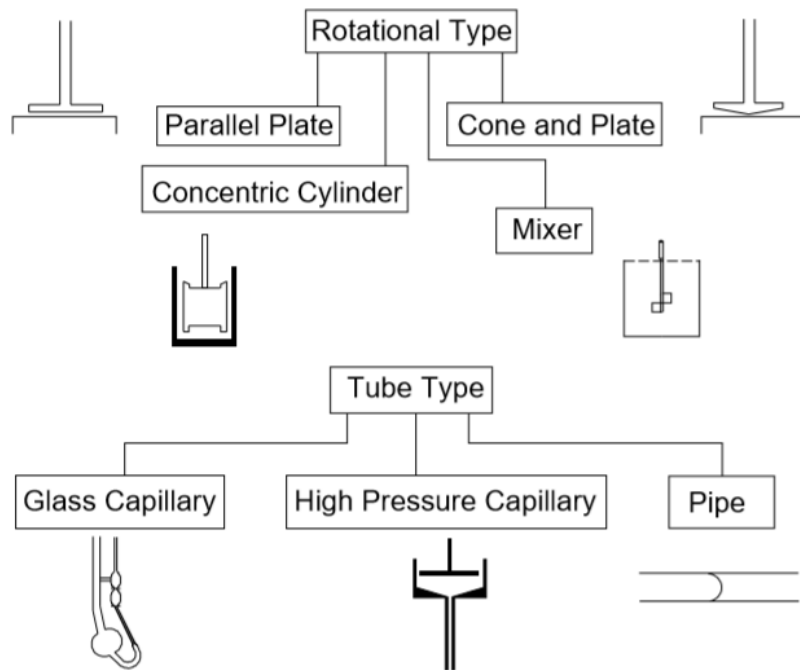


Figure 15: Rotational and tube type rheometers [16]

As all measuring systems, certain limitations are set to each system, for example, some capillaries, like the glass capillary, are only suitable for Newtonian fluids. In addition, parallel plate and cone and plate viscometers can handle the measurement of fluids with particles much smaller than pipe and mixer viscometers [16]. For this thesis, measurement of the rheological properties of collagen are done using a capillary/slit rheometer. This is due to the consistency of investigated material and the range of shear rates in capillary rheometers which is like applications in the process treatment of collagen (pumping, mixing and extrusion). Therefore, the following text covers the flow governing only this type of rheometer.

Capillary rheometers, due to their simplicity and similarity to many process applications like flow through pipes, are the most used. They can also be converted to produce slit and annular flows [18]. Capillary rheometers can be divided into two groups: plunger-type capillary rheometers and continuous-flow capillary rheometers. Both rheometers have a capillary die, however, plunger-type capillary rheometers can only measure shear viscosity [25]. Both types are shown in figure 16 and figure 17.

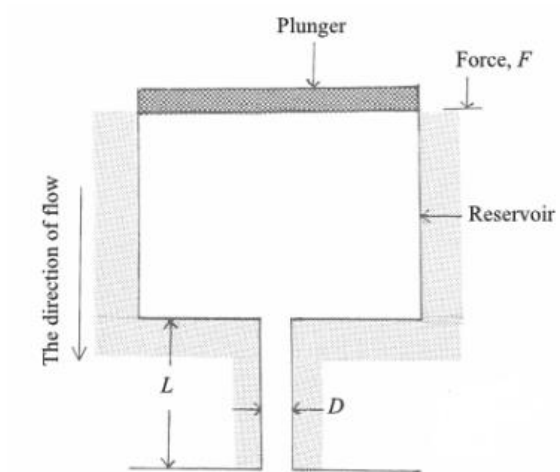


Figure 16: Plunger-type capillary rheometer [25]

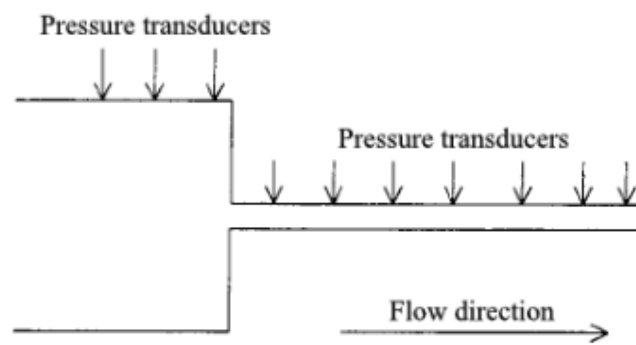


Figure 17: Continuous-flow capillary rheometer [25]

2.4.1 Slit Rheometry

The technology of slit rheometers has been used in practice since the early 1960's. Because pressure transducers are mounted directly above the die wall in a slit die, the pressure drop can be precisely measured along the die length. In addition, the range of shear rate is broader, and slits can be easily constructed in processing facilities [16].

Consequently, slit rheometry facilitates measurements of the rheological properties of complicated materials [26]. Length L , width w , and height h are used to describe slit size. Another important parameter is a slit's aspect ratio or width-to-height ratio. In slit rheometers, the aspect ratio must be greater than 10 to neglect edge effects [16]. Figure 18 shows a general sketch of a slit rheometer.

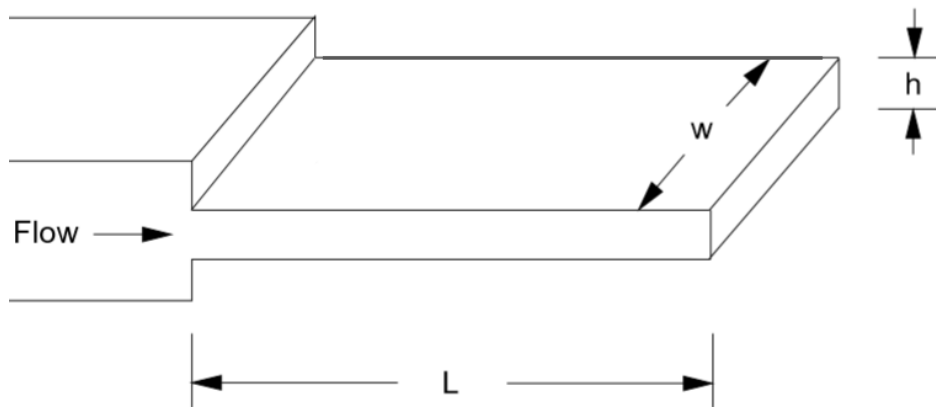


Figure 18: Slit rheometer [16]

The flow in slit and capillary rheometers will be assumed to be laminar given the high viscosities often encountered when dealing with non-Newtonian fluids. The following set of equations described in resource [18] account for flow in capillary rheometers. To determine the shear stress at the wall of a tube, equation (14) is used:

$$\tau_w = \frac{\Delta P \cdot R}{2L} \quad (14)$$

where:

τ_w [Pa] is wall shear stress

ΔP [Pa] is pressure drop

R [m] is radius of circular tube

L [m] is tube length

The Hagen-Poiseuille equation, used for Newtonian fluids to determine the mean velocity V , is shown in equation (15):

$$V = \left(\frac{\Delta P}{L}\right) \left(\frac{R^2}{8\eta}\right) \quad (15)$$

Rearranging equation (15) in terms of equation (14) gives the wall shear stress:

$$\left(\frac{\Delta P}{L}\right) \left(\frac{R}{2}\right) = \tau_w = \eta \left(\frac{8V}{D}\right) \quad (16)$$

where:

V [m/s] is the mean velocity

D [m] is tube diameter

Since equation (16) evidently describes Newtonian fluid behaviour, where the shear rate is,

$$\dot{\gamma} = \frac{8V}{D} \quad (17)$$

an additional correction factor must be added to determine the shear rate for non-Newtonian fluids. However, this shear rate is generally used for non-Newtonian fluids as a nominal or apparent shear rate at the wall. The mean velocity can also be found using the flow rate Q as shown in the equation (18):

$$V = \frac{Q}{\pi R^2} \quad (18)$$

where:

Q [m³/s] is volumetric flow rate

Substituting equation (18) into equation (17), the shear rate for the flow through capillary can be approximated using the following equation:

$$\dot{\gamma} = \frac{4 \cdot Q}{\pi R^3} \quad (19)$$

Since equations (14) through (19) describe flow through tubes, it is necessary to introduce the hydraulic diameter to account for the flow in other cross-sections. Hence, when working with non-circular flow, the hydraulic diameter, described below, replaces the instances where the radius R is used [18].

$$D_h = \frac{\text{four times the area of the flow}}{\text{wetted perimeter}}$$

where, for the flow through a rectangular slit:

$$D_h = \frac{4 \cdot h \cdot w}{2(h+w)} \quad (20)$$

Then,

$$R = \frac{D_h}{2} \quad (21)$$

where:

h [m] is the height of capillary

w [m] is the width of capillary

2.5 Summary of Literature Review

The first section of the literature review dealt with collagen and three model fluids known as CMC, PAA and M1. Collagen is a fibrous, hard, insoluble, and structural protein made up of amino acids. It is the most abundant protein in all mammals. Collagen can be extracted from bovine, porcine, and fishes. Due to collagen's complex structure and its various uses in the industry, scientists from several sectors have been studying the mechanical properties of collagen solutions using numerous methods to model its viscoelastic behaviour. On the other hand, PAA solutions, which are exceptional engineering polymers exhibiting viscoelastic behaviour and are used in microelectronics, were later discussed along with CMC and M1. Carboxymethyl cellulose (CMC) is a non-toxic cellulose derivative used in countless industries. Lastly, M1 is a test fluid developed at Monash University to unify rheological measurements. These model fluids are commonly used to validate rheometer experiments.

Sections 2.3-2.3.7 of the literature review dealt with the basics of flow and deformation, the classification of fluids as well as equations modelling fluid behaviour. Primarily, Newtonian fluids, non-Newtonian fluids which are subdivided into time-independent fluids, time-dependent fluids, and finally viscoelastic fluids. Several empirical relations have been developed to model fluid behaviour like the power-law or Ostwald-de Waele model, the Cross model, the Bingham plastic model, and many others. Of these models, the power-law model stands out as a simple two-parameter equation commonly preferred by scientists for modelling the behaviour of many non-Newtonian fluids apart from very low shear rates. Finally, viscoelasticity and its effects were discussed. From jet swelling to the tubeless siphon and Weissenberg effects, viscoelastic materials exhibit unusual flow phenomena.

The final section dealt with rheometry: the experimental methods used by scientists to measure rheological properties of materials. Capillary rheometers, given their simplicity in manufacturing, versatility, and similarity to many practical applications, were the focus of this section. Capillary rheometers can also be easily equipped and altered to produce slit flows. Finally, equations governing the flow in slit and capillary rheometers were discussed. The equations accounted for modelling of rheological data through a capillary however with certain alterations can be used to model flow through a slit.

Collagen material, shown in Figure 20, is evidently a white and pasty substance with a behaviour resembling dough. According to reference [40], a recent study done on the rheological properties of collagen in aqueous dispersions suggests that an increase in

temperature accompanied by an increase in shear rates results in a substantial decrease in viscosity. On the other hand, when stopping the shear and gradually decreasing the temperature, the collagen solution exhibits thixotropic behaviour with a partial time-dependent viscosity recovery [40]. The study also suggests that when shear rates were increased to 3000 s^{-1} , the viscosity of the collagen dispersion decreased by 700 times its original value and recovered 91 % of its initial viscosity ten seconds upon returning the shear rate to its original value [40].

Another study on acylated pepsin-solubilized collagen extracted from calf skin shows the typical pseudoplastic behaviour of collagen [41]. When modelled using the power-law, native collagen was used as a model fluid and was found to have a power law index of $n = 0.42$ [41].

Given the circumstances in which this thesis was written (2020 pandemic), experimental measurements of the three model fluids were eliminated. Therefore, the following experiments will aim at finding the rheological properties of collagen material using the power-law model and a capillary rheometer equipped with a slit die.

3 Experiments

This chapter deals with the methodology, equipment and data processing of the experiments performed on collagen to determine its rheological properties using the power-law model. The sample investigated is a water-collagen solution with a measured dry content of 9.69 %. The bovine-extracted collagen was kept refrigerated at a temperature of 9 °C until the experiments were performed. The collagen sample, stored in an air-tight bag, is shown in figure 20.

The experimental apparatus is a capillary rheometer equipped with a slit die. The extrusion capillary rheometer, shown in figure 21, was constructed at the Czech Technical University in Prague. In addition, three slit dies which are used in this measurement, were also manufactured on-campus. The extrusion rheometer consists of a capillary, investigated material storage cylinder, and a piston powered by a hydraulic unit all mounted on a steel frame [38]. The capillary is equipped with five pressure transducers while a sixth transducer is mounted into the storage cylinder [39]. The scheme of the experiment is shown in the figure below:

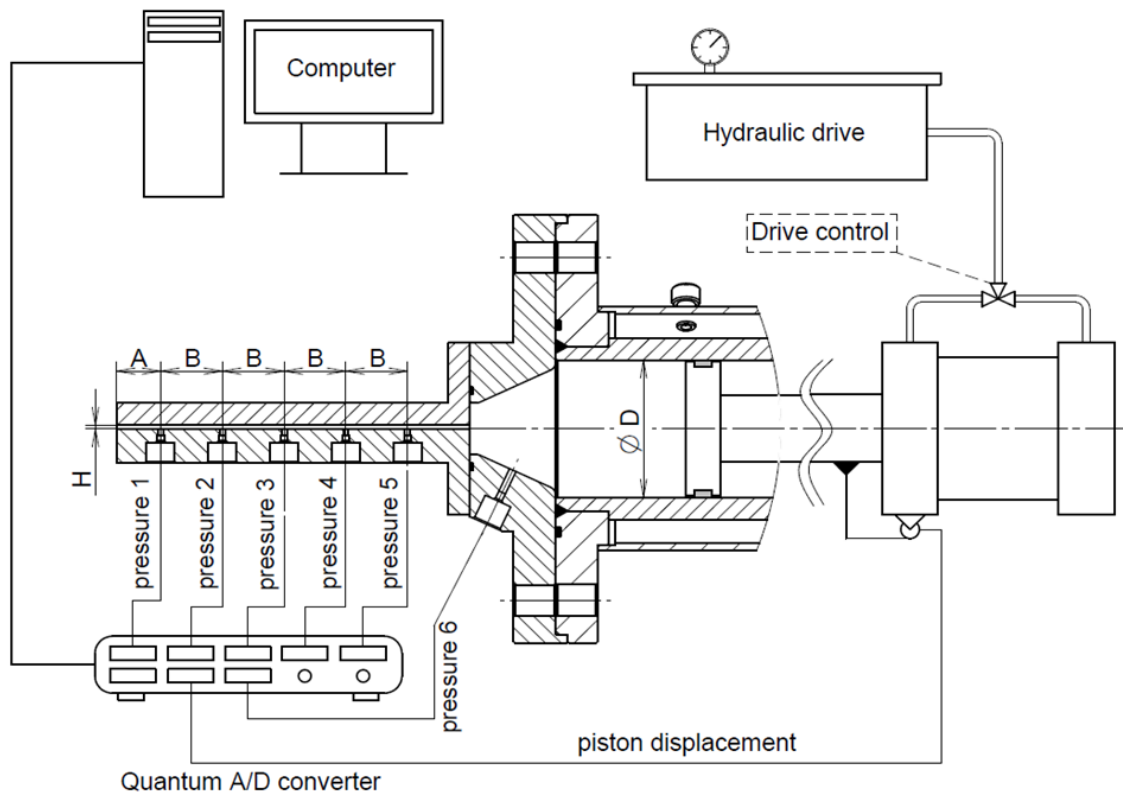


Figure 19: Scheme of the capillary rheometer apparatus where $A=25$ mm, $B= 35$ mm and $D= 80$ mm [39]



Figure 20: Collagen sample

As seen in figure 19, the pressure transducers are mounted on the bottom part of the die while the top part is removeable to allow for bolting of slit dies with different geometries. All sensors are connected to a universal data acquisition system QuantumX MX840B and the software for data acquisition was developed in LabVIEW [39]. The transducers are separated by distance B , while the first transducer (measuring pressure 1) is 25 mm away from the edge of the capillary. The width of the capillary is evidently constant, and the length of the capillary is $L = 200$ mm. The dimensions of the slits used in the experiment are shown in table 1. In addition, the hydraulic diameter, which will be used in data processing is calculated for each slit.

	Width [mm]	Height [mm]	Hydraulic Diameter [mm]
Capillary 1	20	8	11.43
Capillary 2	20	4	6.67
Capillary 3	20	2	3.64

Table 1: Capillary dimensions

Evidently, in the case of capillary 3, the aspect ratio is equal to 10. Therefore, according to [16], measured data correction to account for the effects of side edges of capillary must be considered.



Figure 21: Capillary rheometer used for experimental measurements

Figure 22 shows (from left to right) capillaries 3, 2, and 1, respectively. It is important to note that, given the apparatus design, refilling the collagen into the cylindrical section did not require the removal of the then-used slits as it can be refilled from the rear part [39].



Figure 22: Slit dies used in the extrusion capillary rheometer

3.1 Method of Measurement

First, the ambient conditions were measured where the external temperature was $T_{external} = 13\text{ }^{\circ}\text{C}$ and the internal lab temperature was $T_{lab} = 22\text{ }^{\circ}\text{C}$. The humidity was at 77 % and the pressure was 1014 hectopascals.

Prior to the experiment, the cylindrical portion of the rheometer, in addition to the piston, slits, and the sealing elements were all cleaned from the collagen residue left-over from previous measurements. Then, capillary 1 (dimensions 20 mm x 8 mm) was installed. The collagen was then taken out from the refrigerator and, using a thermometer, its temperature was measured at 9 °C.

The piston was initially moved back to the bottom-dead centre and the collagen was manually refilled into the cylindrical portion. At the same time, the signal from the transducers was tested and all the measured data were set to 'zero'. The first experiment, immediately after switching to a different slit die, was used to fill up the capillary with the investigated material in preparation for the factual measurement. The experiment commenced with the movement of the hydraulically driven piston from the bottom-dead centre and was only stopped after the piston reached the top-dead centre. The extruded collagen was collected, and it was not further re-used. The extruded collagen's temperature was measured at 12.5 °C.

Collagen extrusion through capillary 1 was done seven times with a gradually increasing piston velocity to ensure that the required shear range is covered. Therefore, in the case of capillary 1, three experiments were done for velocity 1, and one experiment each for velocity 2 through velocity 5.

Throughout the experiment, the piston position as well as pressure recordings from the five strain gauges were measured at a time step of 10 millisecond. The duration of each extrusion took no longer than 15 seconds with greater piston velocities resulting in less extrusion times. The piston position is recorded using a linear potentiometric sensor (Micro-epsilon, WPS-500) [38]. In the case of capillaries 2 and 3, the amount of collagen material required for the experiment was underestimated. Therefore, in addition to the preliminary experiment required to fill the slit dies, only one measurement for each velocity (velocities 1 to 5) was done.

In certain cases, when the investigated material was being extruded, a large amount of air bubbles caused by collagen refilling necessitated repeating the experiment. Nevertheless, the process of cutting collagen into smaller pieces for filling the cylinder

would inevitably cause air bubbles throughout every extrusion. Figure 23 shows collagen being extruded through capillary 2 (dimensions 20 mm x 4 mm).



Figure 23: Collagen extrusion through capillary slit rheometer

The number of experiments performed corresponding to each capillary and velocity is illustrated in table 2. Furthermore, three additional experiments, by using capillary 3 (dimensions 20 mm x 2 mm) and velocities 1, 3, and 5, were done to study the behaviour of re-extruded collagen. Prior to re-extrusion, the temperature of collagen was measured at 14 °C, while after re-extrusion the collagen's temperature was recorded at 15.5 °C.

	Velocity 1	Velocity 2	Velocity 3	Velocity 4	Velocity 5
Capillary 1	3	1	1	1	1
Capillary 2	1	1	2	1	1
Capillary 3	1	1	1	2	1

Table 2: Number of experiments performed using each capillary and the corresponding velocity

3.2 Method of Data Processing

After finalizing the experiments, the extracted data is processed using MATLAB R2017a. Before processing, it is important to note the data files, shown in figure 24, resulting from the experiments. Each file contains 9 columns; the first and last (not shown in figure 24) columns are the absolute time, while the pressure recordings P1 through P6, in bars, are found in the second until the sixth columns, respectively. The eighth column shows the piston position recorded in millimetres.

3813,47735	-0,00163	0,00050	0,00148	-0,00142	0,00102	-0,00184	0,33016
3813,48734	-0,00361	0,00056	0,00116	-0,00123	0,00129	-0,00176	0,33024
3813,49734	-0,00185	0,00040	0,00147	-0,00117	0,00148	-0,00171	0,33030
3813,50734	-0,00380	0,00026	0,00192	-0,00125	0,00157	-0,00167	0,33026
3813,51733	-0,00177	0,00019	0,00175	-0,00131	0,00151	-0,00177	0,33019
3813,52733	-0,00357	-0,00001	0,00139	-0,00135	0,00142	-0,00191	0,33017
3813,53733	-0,00182	-0,00024	0,00142	-0,00149	0,00135	-0,00190	0,33017
3813,54733	-0,00400	-0,00034	0,00122	-0,00146	0,00129	-0,00174	0,33017
3813,55732	-0,00205	-0,00022	0,00077	-0,00150	0,00106	-0,00166	0,33013
3813,56732	-0,00405	-0,00018	0,00072	-0,00164	0,00099	-0,00169	0,33009
3813,57732	-0,00199	-0,00030	0,00133	-0,00171	0,00086	-0,00171	0,33009
3813,58732	-0,00405	-0,00034	0,00200	-0,00136	0,00072	-0,00159	0,33010
3813,59731	-0,00234	-0,00019	0,00218	-0,00100	0,00059	-0,00153	0,33011
3813,60731	-0,00454	0,00006	0,00216	-0,00091	0,00055	-0,00132	0,33016
3813,61731	-0,00254	0,00017	0,00204	-0,00118	0,00049	-0,00135	0,33012
3813,62731	-0,00457	0,00031	0,00166	-0,00149	0,00052	-0,00140	0,33007
3813,63730	-0,00236	0,00043	0,00119	-0,00164	0,00063	-0,00139	0,33013
3813,64730	-0,00428	0,00051	0,00069	-0,00152	0,00081	-0,00133	0,33020
3813,65730	-0,00222	0,00053	0,00030	-0,00154	0,00082	-0,00132	0,33016
3813,66730	-0,00423	0,00055	0,00017	-0,00147	0,00069	-0,00124	0,33008
3813,67729	-0,00212	0,00044	0,00024	-0,00132	0,00043	-0,00132	0,33005
3813,68729	-0,00440	0,00034	0,00042	-0,00113	0,00025	-0,00134	0,33014
3813,69729	-0,00229	0,00035	0,00064	-0,00113	0,00015	-0,00151	0,33016
3813,70729	-0,00409	0,00033	0,00106	-0,00126	0,00026	-0,00154	0,33018
3813,71728	-0,00179	-0,00002	0,00138	-0,00151	0,00020	-0,00159	0,33016

Figure 24: Example of acquired data after one measurement

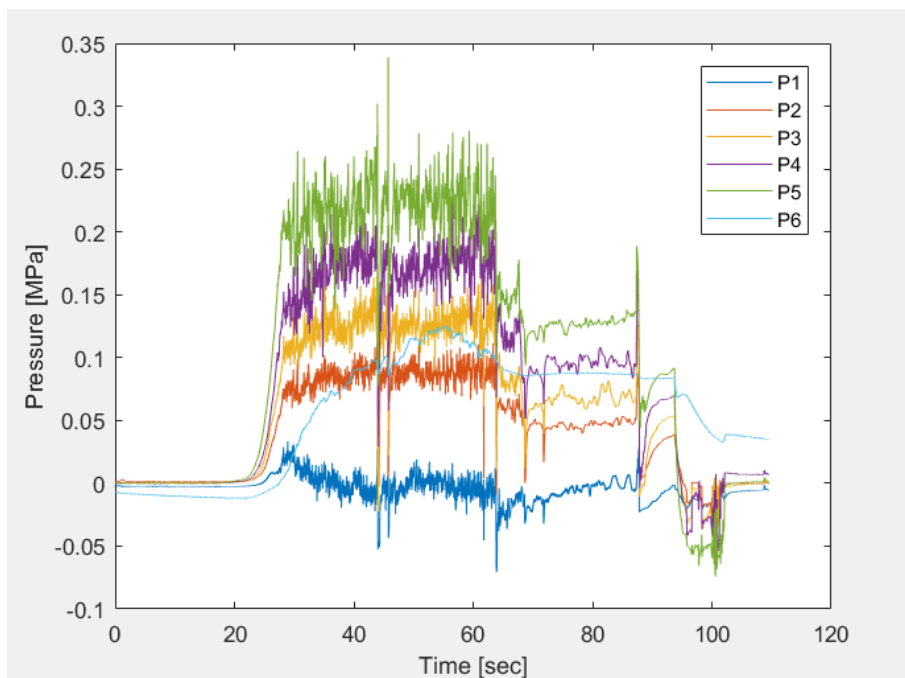


Figure 25: Pressure profiles of the first experiment with capillary 1

First, the data must be imported to MATLAB using the Import Tool, and the absolute time is then converted into time starting from zero seconds with a time step of 0.01 seconds. The graph of the recorded pressures plotted against time is shown in figure 25.

Evidently from figure 25, when determining the rheological properties of the investigated collagen material, data recorded from the start and end of the experiment must be filtered out in MATLAB. To determine the wall shear stress, the evaluation of ΔP will not include the sixth pressure recording from the cylindrical section of the rheometer. Therefore, to find the pressure drop, ΔP , the mean values of $P5$ and $P1$ are first calculated. Figure 26 shows the approximate range from which ΔP is calculated. In this case, ΔP is calculated from the values of $P5 - P2$.

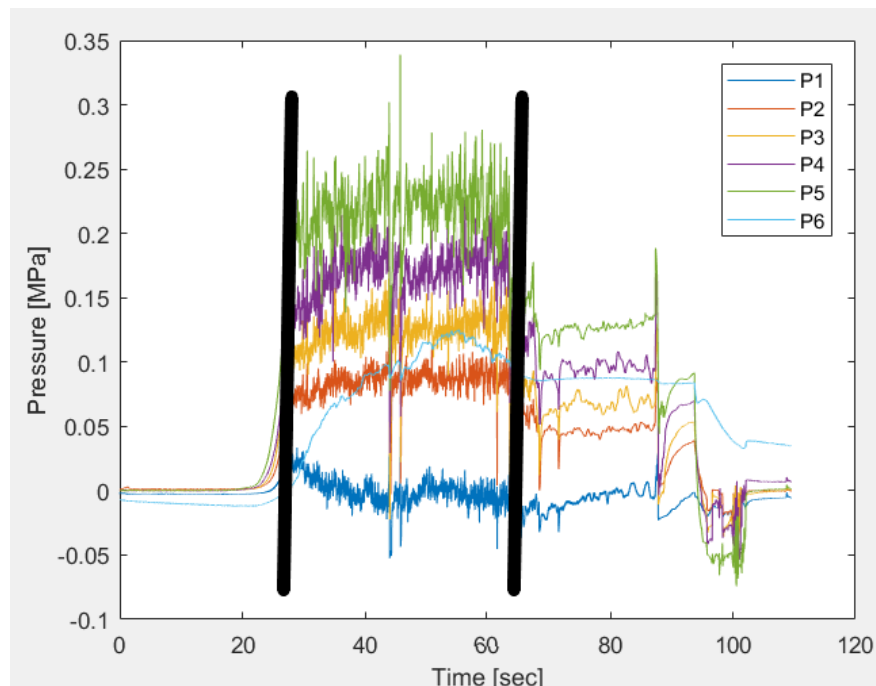


Figure 26: Bold lines specify the approximate range from which the average pressure drop is calculated, capillary 1

Three approaches will be used in data processing from which the power-law results will be obtained. Before applying these methods, the velocity, volumetric flow rate of collagen, and the mean pressure drop must be calculated. An overview of each approach is presented below.

The first approach (hydraulic diameter), based on the equations described in section 2.4.1, transforms the flow through a slit to flow in a straight circular pipe [15]. The shear rate is calculated using equation (14), which must be altered to account for the flow through a slit employing the hydraulic diameter. As shown in table 3, the radius needed in equation (14) must be re-calculated corresponding to each hydraulic diameter.

	Hydraulic Diameter [mm]	Recalculated Radius [mm]
Capillary 1	11.4	5.7
Capillary 2	6.7	3.3
Capillary 3	3.6	1.8

Table 3: Recalculated radius for the flow through a slit

To evaluate the shear rate, the piston velocity must be calculated using the piston position and the time increments. A graph of piston position vs. time is shown in figure 27. The slope is calculated to find the piston velocity from the position-time graph. The resulting velocity is constant, as shown by the constant slope straight line in figure 27. The constant velocity section is in the time interval of approximately 6 to 63 seconds (for velocity 1). Figure 28 shows the resulting velocity by performing a linear regression. In this case, the velocity is approximately $V = 0.00098$ m/s. Figures 27 and 28 are created using data from capillary 1, velocity 1, and experiment 1. As shown in equation (18), the volumetric flow rate can be found by multiplying the piston velocity by its cross-sectional area. The calculated volumetric flow rate of collagen is then used to calculate the shear rate using equation (19). Therefore, from the evaluation of the pressure drop, the corresponding wall shear stresses and shear rates are calculated. Finally, the evaluated points from velocities 1 through 5 create a rheogram of collagen for a specific slit die. MATLAB's data fitting tool is then used to fit the rheogram to a power-law model where the consistency coefficient K [$Pa \cdot s^n$] and the power-law index n [-] are found.

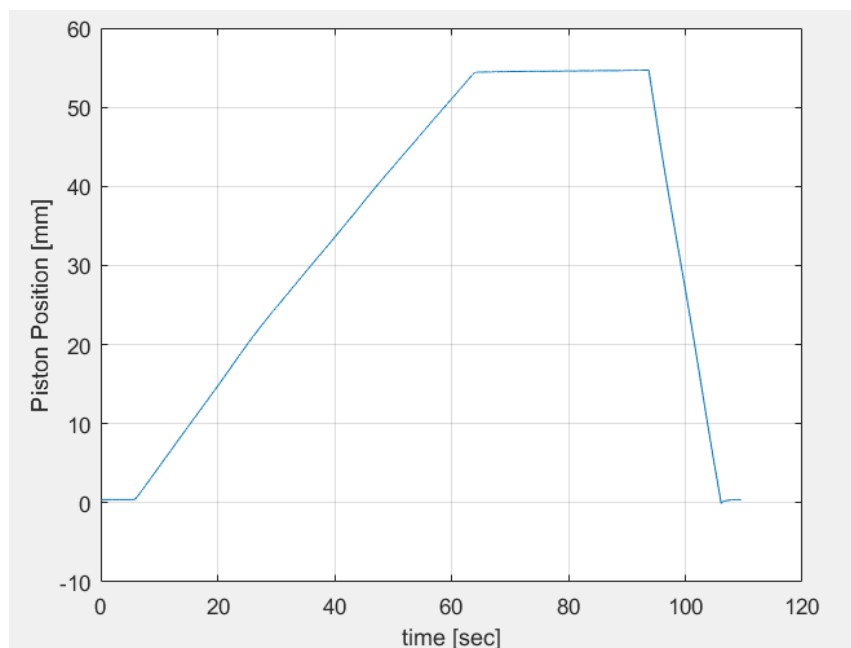


Figure 27: Position of the piston vs. time

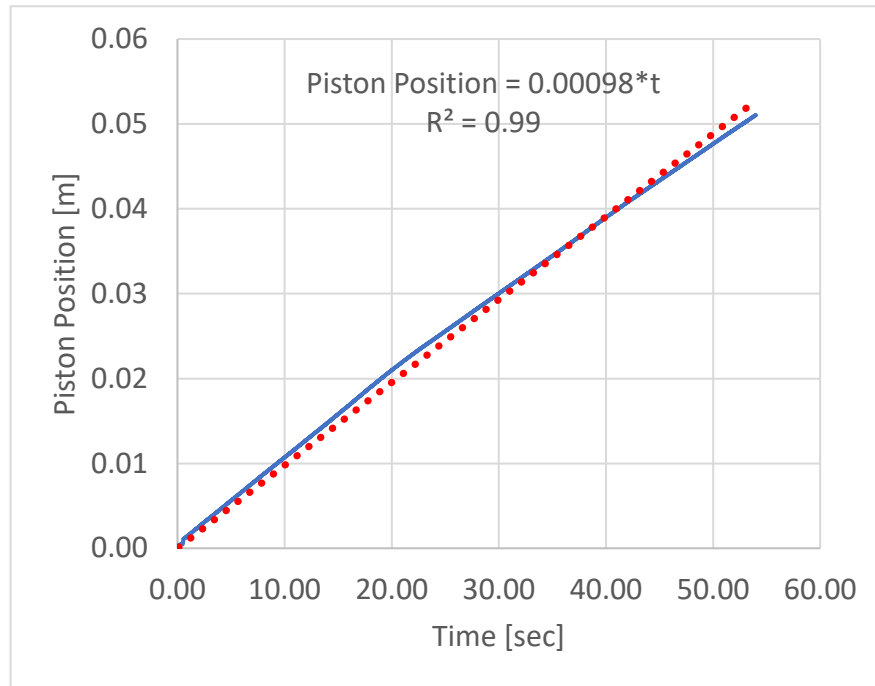


Figure 28: Piston velocity determined by linear regression

Evidently, equation (19) is used to calculate the shear rate for Newtonian fluids. However, since collagen material is non-Newtonian, a second calculation for the non-Newtonian shear rate employing the resulting power-law index n will be done. The aim is to create iterations of shear rate calculations in which the next resulting power-law index is constant to the third decimal. Equation (22) describes the evaluation of the wall shear rate used in the first approach for a power-law fluid [15].

$$\dot{\gamma} = \frac{Q}{\pi R^3} \left[3 + \frac{1}{n} \right] \quad (22)$$

where:

Q [m³/s] is volumetric flow rate

n [-] is power-law index

R [m] is radius of circular tube recalculated using the hydraulic diameter

The second approach (parallel plates) is based on transforming the flow through a slit to flow in a very wide slot [15]. In this case, the volumetric flow rates previously calculated will be first used to calculate the shear rate as shown in equation (23).

$$\dot{\gamma} = \frac{6 \cdot Q}{B \cdot H^2} \quad (23)$$

where:

Q [m³/s] is volumetric flow rate

B and H [m] are the capillary's base and height

Then, the wall shear stress is evaluated using equation (24). Finally, the calculated points are used to create a rheogram from which the power-law index and consistency coefficient are found using MATLAB's data fitting tool. Like the first approach, the second approach also includes finding the power-law index in iterations using equation (25), which describes the calculation of shear rate for a power-law fluid in case of the flow through a very wide slot.

$$\tau_w = \frac{\Delta P \cdot H}{2L} \quad (24)$$

where:

τ_w [Pa] is wall shear stress

ΔP [Pa] is pressure drop

H [m] is height of capillary

L [m] is the distance at which ΔP is calculated

$$\dot{\gamma} = \frac{2 \cdot Q}{B \cdot H^2} \left[2 + \frac{1}{n} \right] \quad (25)$$

where:

Q [m³/s] is volumetric flow rate

n [-] is power-law index

B and H [m] are the capillary's base and height

The third approach (rectangular slit), which is used for a power-law fluid in non-circular ducts, is based on fitting the resulting wall shear stresses to equation (26) [18]. First, the wall shear stress is found using equation (14). Then, for each capillary, the resulting points are plotted against the collagen velocities. Equation (26) is then used to create a fit where the power-law index and the consistency coefficient are found.

$$\tau_w = K \left(\frac{8 \cdot V}{D_h} \left(b + \frac{a}{n} \right) \right)^n \quad (26)$$

where:

τ_w [Pa] is wall shear stress

K [Pa.sⁿ] is consistency coefficient

V [m/s] is the velocity of collagen

D_h [m] is the hydraulic diameter

n [-] is power-law index

The quantities a [-] and b [-] are geometric parameters which characterise the duct's cross-section [18]. Figure 29 shows typical values of these parameters for rectangular ducts. By interpolation, the resulting values of a and b for capillaries 1, 2, and 3 are shown in table 4.

$E = H/W$	a	b
0.00	0.5000	1.0000
0.25	0.3212	0.8182
0.50	0.2440	0.7276
0.75	0.2178	0.6866
1.00	0.2121	0.6766

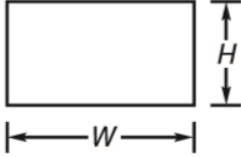


Figure 29: Typical values of a and b [18]

Capillary Number	H/W [-]	a [-]	b [-]
Capillary 1	8/20 = 0.4	0.2749	0.7638
Capillary 2	4/20 = 0.2	0.3569	0.8546
Capillary 3	2/20 = 0.1	0.4284	0.9273

Table 4: Values of a and b recalculated for capillaries 1, 2, and 3

3.3 Results and Discussion

Using the three approaches of data processing described in section 3.2, the results from the experiments on the investigated collagen material with a dry content of 9.69 % are presented in this section. Beginning with the first approach (hydraulic diameter), table 5 outlines the results of the zeroth iteration for capillary 1. The evaluated wall shear stresses, shear rates (calculated for the Newtonian case), piston velocity, mean pressure drop, and volumetric flow rate of collagen are also shown. In addition, the distance at which ΔP is calculated, denoted by L [m], is also shown. Table 6 shows the results of the first iteration, with recalculated values of shear rate using the resulting power-law index obtained from the zeroth iteration.

Capillary 1 (dimensions 20 mm x 8 mm) – 0th Iteration						
Velocity	ΔP [MPa]	L [m]	v [m/s]	Q [m ³ /s]	τ_w [MPa]	$\dot{\gamma}_N$ [1/s]
1	0.133	0.105	0.00098	4.91x10 ⁻⁶	0.0036	33.5
1	0.134	0.105	0.0010	5.05x10 ⁻⁶	0.0037	34.5
1	0.142	0.105	0.0010	5.03x10 ⁻⁶	0.0039	34.3
2	0.159	0.105	0.0023	1.18x10 ⁻⁵	0.0043	80.3
3	0.208	0.105	0.0092	4.63x10 ⁻⁵	0.0056	315.9
4	0.205	0.105	0.0087	4.38x10 ⁻⁵	0.0056	299.1
5	0.221	0.105	0.017	8.61x10 ⁻⁵	0.006	587.2

Table 5: Results of the zeroth iteration for capillary 1 using the first approach

Capillary 1 (dimensions 20 mm x 8 mm) – 1st Iteration						
Velocity	ΔP [MPa]	L [m]	v [m/s]	Q [m ³ /s]	τ_w [MPa]	$\dot{\gamma}_{NN}$ [1/s]
1	0.133	0.105	0.00098	4.91x10 ⁻⁶	0.0036	72.7
1	0.134	0.105	0.0010	5.05x10 ⁻⁶	0.0037	74.8
1	0.142	0.105	0.0010	5.03x10 ⁻⁶	0.0039	74.5
2	0.159	0.105	0.0023	1.18x10 ⁻⁵	0.0043	174.2
3	0.208	0.105	0.0092	4.63x10 ⁻⁵	0.0056	685.3
4	0.205	0.105	0.0087	4.38x10 ⁻⁵	0.0056	648.9
5	0.221	0.105	0.017	8.61x10 ⁻⁵	0.006	1274

Table 6: Results of the first iteration for capillary 1 using the first approach

Evidently, in the case of the first approach, the difference between the zeroth and first iterations is in the recalculation of the Newtonian shear rate $\dot{\gamma}_N$, to the non-Newtonian shear rate $\dot{\gamma}_{NN}$. Table 7 shows the resulting power law index and consistency coefficient for capillary 1 using the first approach. Furthermore, the values of the coefficient of determination suggesting the goodness of fit are also shown. Figure 30 shows the resulting rheograms obtained from the data in tables 5 and 6.

Capillary 1 Results			
Iteration Number	n [-]	K [Pa.s ⁿ]	R^2
0	0.18	2006	0.9879
1	0.18	1751	0.9879

Table 7: Power-law results for capillary 1 using the first approach

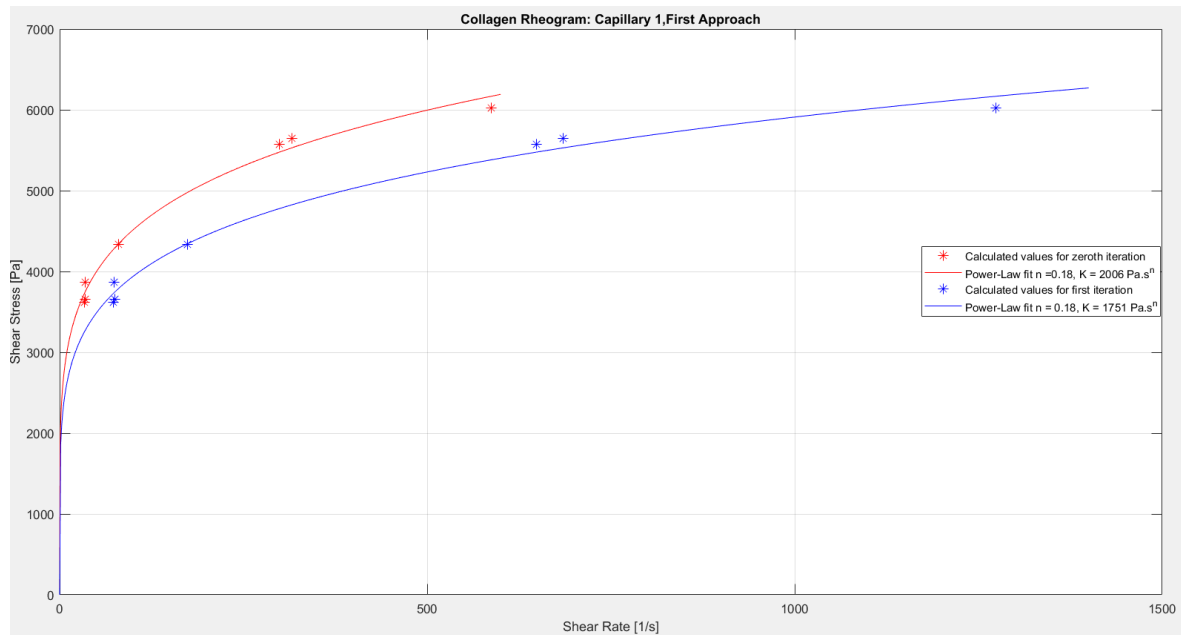


Figure 30: Comparison of the resulting rheograms for capillary 1 using the first approach

The results of the zeroth and first iterations for capillary 2 using the first approach are shown in tables 8 and 9, respectively. The results of the power-law fit are shown in table 10. Figure 31 shows the resulting rheograms obtained from the data in tables 8 and 9.

Capillary 2 (dimensions 20 mm x 4 mm) – 0 th Iteration						
Velocity	ΔP [MPa]	L [m]	v [m/s]	Q [m ³ /s]	τ_w [MPa]	$\dot{\gamma}_N$ [1/s]
1	0.29	0.105	0.00098	4.93×10^{-6}	0.0046	169.6
2	0.341	0.105	0.0028	1.39×10^{-5}	0.0054	478.2
3	0.484	0.105	0.0098	4.94×10^{-5}	0.0077	1698.6
3	0.498	0.105	0.0099	4.96×10^{-5}	0.0079	1704.6
4	0.497	0.105	0.010	5.03×10^{-5}	0.0079	1731.2
5	0.474	0.105	0.016	7.92×10^{-5}	0.0075	2724.3

Table 8: Results of the zeroth iteration for capillary 2 using the first approach

Capillary 2 (dimensions 20 mm x 4 mm) – 1 st Iteration						
Velocity	ΔP [MPa]	L [m]	v [m/s]	Q [m ³ /s]	τ_w [MPa]	$\dot{\gamma}_{NN}$ [1/s]
1	0.29	0.105	0.00098	4.93×10^{-6}	0.0046	330.2
2	0.341	0.105	0.0028	1.39×10^{-5}	0.0054	930.9
3	0.484	0.105	0.0098	4.94×10^{-5}	0.0077	3306.8
3	0.498	0.105	0.0099	4.96×10^{-5}	0.0079	3318.5
4	0.497	0.105	0.010	5.03×10^{-5}	0.0079	3370.1
5	0.474	0.105	0.016	7.92×10^{-5}	0.0075	5303.5

Table 9: Results of the first iteration for capillary 2 using the first approach

Capillary 2 Results			
Iteration Number	n [-]	K [Pa.s^{n}]	R^2
0	0.21	1579	0.9052
1	0.21	1374	0.9052

Table 10: Power-law results for capillary 2 using the first approach

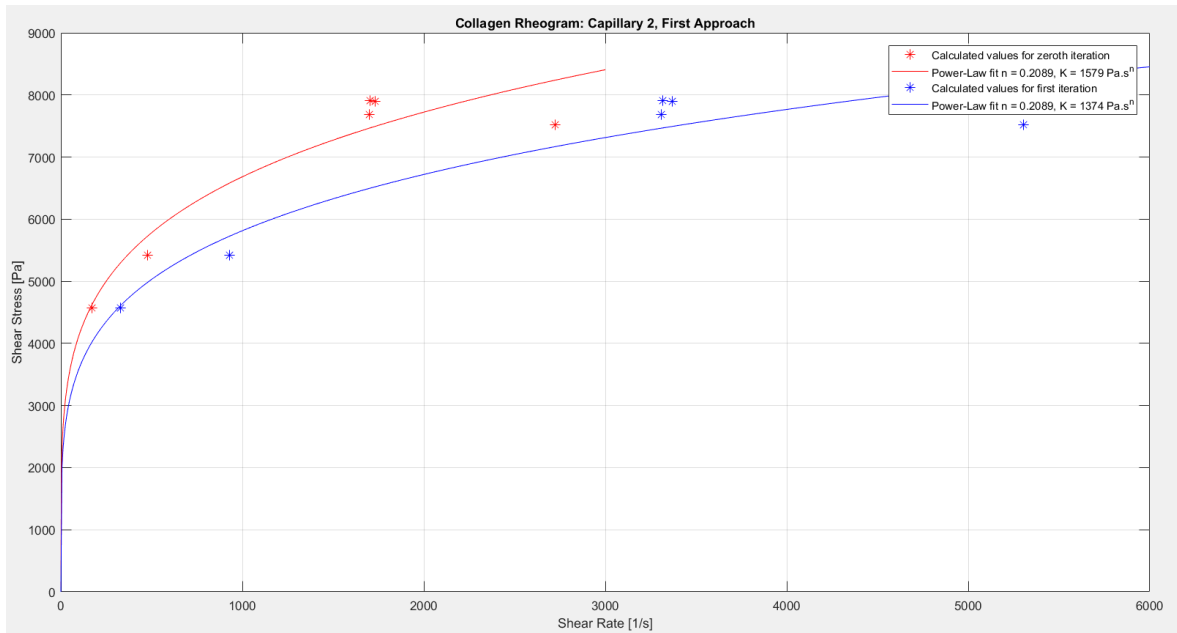


Figure 31: Comparison of the resulting rheograms for capillary 2 using the first approach

Similarly, tables 11, 12, and 13 outline the results of the first approach for capillary 3. Figure 32 shows the resulting rheogram.

Capillary 3 (dimensions 20 mm x 2 mm) – 0th Iteration						
Velocity	ΔP [MPa]	L [m]	v [m/s]	Q [m³/s]	τ_w [MPa]	$\dot{\gamma}_N$ [1/s]
1	0.579	0.105	0.00089	4.47×10^{-6}	0.005	946.3
2	0.755	0.105	0.0025	1.27×10^{-5}	0.0065	2695.7
3	0.951	0.105	0.0053	2.66×10^{-5}	0.0082	5625.4
4	-	-	-	-	-	-
4	1.059	0.105	0.0095	4.75×10^{-5}	0.0092	10067.9
5	1.152	0.105	0.016	8.24×10^{-5}	0.0099	17460.7

Table 11: Results of the zeroth iteration for capillary 3 using the first approach.
Experiment 1 with velocity 4 had unusable data due to stopping the piston movement during the measurement

Capillary 3 (dimensions 20 mm x 2 mm) – 1st Iteration						
Velocity	ΔP [MPa]	L [m]	v [m/s]	Q [m³/s]	τ_w [MPa]	$\dot{\gamma}_{NN}$ [1/s]
1	0.579	0.105	0.00089	4.47×10^{-6}	0.005	1726.3
2	0.755	0.105	0.0025	1.27×10^{-5}	0.0065	4917.9
3	0.951	0.105	0.0053	2.66×10^{-5}	0.0082	10262.6
4	-	-	-	-	-	-
4	1.059	0.105	0.0095	4.75×10^{-5}	0.0092	18367.3
5	1.152	0.105	0.016	8.24×10^{-5}	0.0099	31854.3

Table 12: Results of the first iteration for capillary 3 using the first approach

Capillary 3 Results			
Iteration Number	n [-]	K [Pa.s^{n}]	R^2
0	0.23	1055	0.9833
1	0.23	918	0.9833

Table 13: Power-law results for capillary 3 using the first approach

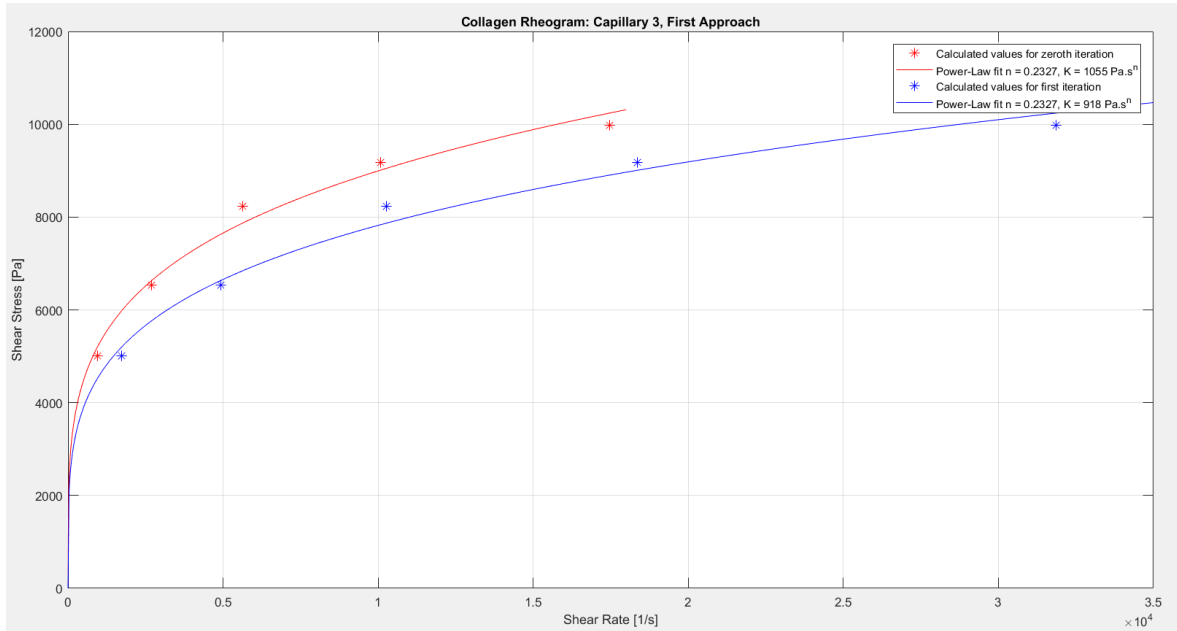


Figure 32: Comparison of the resulting rheograms for capillary 3 using the first approach

Finally, the results of re-extruded collagen through capillary 3 are shown in tables 14, 15, and 16. Figure 33 shows the rheogram of re-extruded collagen.

Re-extruded Collagen Capillary 3 – 0th Iteration						
Velocity	ΔP [MPa]	L [m]	v [m/s]	Q [m³/s]	τ_w [MPa]	$\dot{\gamma}_N$ [1/s]
1	0.539	0.105	0.00083	4.16×10^{-6}	0.0047	880.1
3	0.895	0.105	0.0058	2.9×10^{-5}	0.0078	6134.9
5	1.071	0.105	0.013	6.77×10^{-5}	0.0093	14347.1

Table 14: Results of the zeroth iteration for capillary 3 using the first approach and re-extruded collagen

Re-extruded Collagen Capillary 3 – 1st Iteration						
Velocity	ΔP [MPa]	L [m]	v [m/s]	Q [m³/s]	τ_w [MPa]	$\dot{\gamma}_{NN}$ [1/s]
1	0.539	0.105	0.00083	4.16×10^{-6}	0.0047	1563.3
3	0.895	0.105	0.0058	2.9×10^{-5}	0.0078	10897.2
5	1.071	0.105	0.013	6.77×10^{-5}	0.0093	25484.4

Table 15: Results of the first iteration for capillary 3 using the first approach and re-extruded collagen

Re-extruded Collagen Capillary 3 Results			
Iteration Number	n [-]	K [Pa.s^{n}]	R^2
0	0.24	908	0.997
1	0.24	790	0.997

Table 16: Power-law results for capillary 3 using the first approach and re-extruded collagen

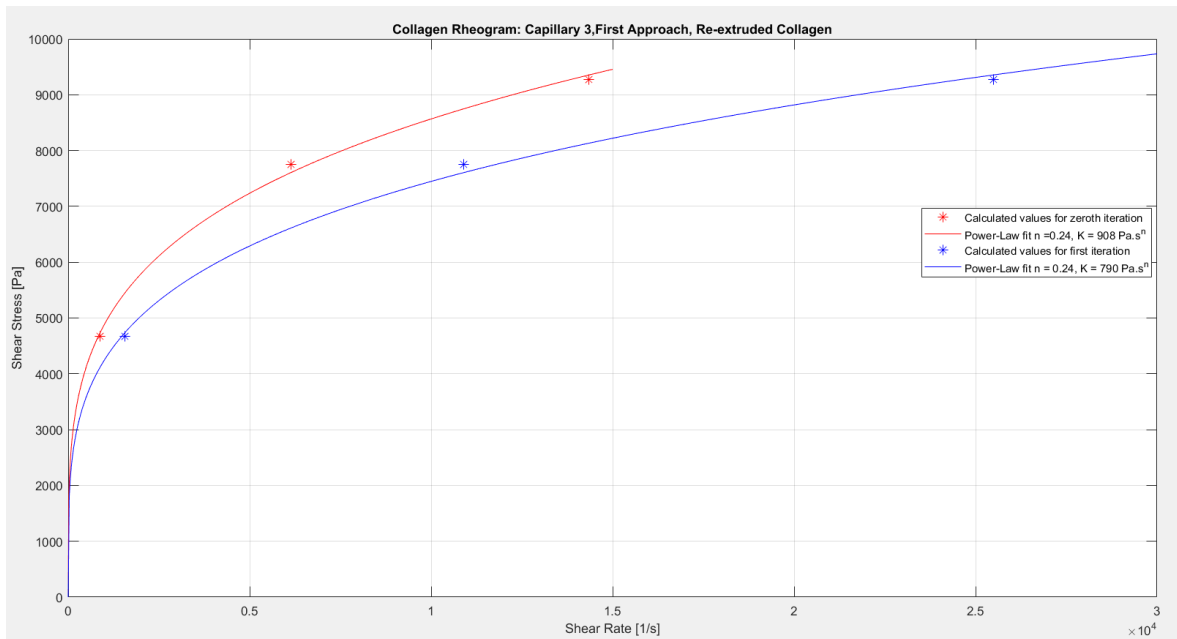


Figure 33: Comparison of the resulting rheograms for capillary 3 using the first approach and re-extruded collagen

Next, the results of the second approach (parallel plates) for each capillary are shown. As previously stated, the wall shear stress and shear rates are recalculated for the flow in a very wide slot. Tables 17, 18, and 19 show the results of capillary 1 using the second approach. Figure 34 shows the resulting rheogram and power-law fit from both iterations for capillary 1.

Capillary 1 (dimensions 20 mm x 8 mm) – 0 th Iteration						
Velocity	ΔP [MPa]	L [m]	v [m/s]	Q [m ³ /s]	τ_w [MPa]	$\dot{\gamma}_N$ [1/s]
1	0.133	0.105	0.00098	4.91x10 ⁻⁶	0.0051	23.02
1	0.134	0.105	0.0010	5.05x10 ⁻⁶	0.0051	23.7
1	0.142	0.105	0.0010	5.03x10 ⁻⁶	0.0054	23.6
2	0.159	0.105	0.0023	1.18x10 ⁻⁵	0.0061	55.1
3	0.208	0.105	0.0092	4.63x10 ⁻⁵	0.0079	217
4	0.205	0.105	0.0087	4.38x10 ⁻⁵	0.0078	205.5
5	0.221	0.105	0.017	8.61x10 ⁻⁵	0.0084	403.4

Table 17: Results of the zeroth iteration for capillary 1 using the second approach

Capillary 1 (dimensions 20 mm x 8 mm) – 1 st Iteration						
Velocity	ΔP [MPa]	L [m]	v [m/s]	Q [m ³ /s]	τ_w [MPa]	$\dot{\gamma}_{NN}$ [1/s]
1	0.133	0.105	0.00098	4.91x10 ⁻⁶	0.0051	58.9
1	0.134	0.105	0.0010	5.05x10 ⁻⁶	0.0051	60.6
1	0.142	0.105	0.0010	5.03x10 ⁻⁶	0.0054	60.4
2	0.159	0.105	0.0023	1.18x10 ⁻⁵	0.0061	141.1
3	0.208	0.105	0.0092	4.63x10 ⁻⁵	0.0079	555.4
4	0.205	0.105	0.0087	4.38x10 ⁻⁵	0.0078	525.9
5	0.221	0.105	0.017	8.61x10 ⁻⁵	0.0084	1032.4

Table 18: Results of the first iteration for capillary 1 using the second approach

Capillary 1 Results			
Iteration Number	n [-]	K [Pa.sⁿ]	R^2
0	0.18	3001	0.9879
1	0.18	2543	0.9879

Table 19: Power-law results for capillary 1 using the second approach

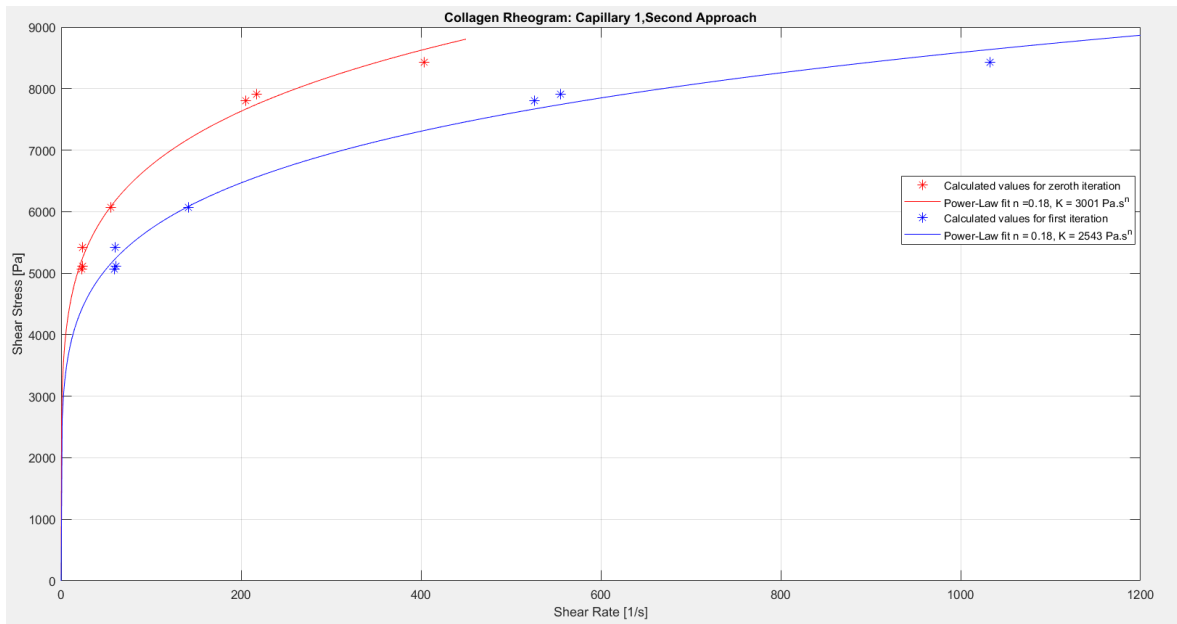


Figure 34: Comparison of the resulting rheograms for capillary 1 using the second approach

Correspondingly, tables 20, 21, and 22 show the second approach (parallel plates) results of capillary 2. Figure 35 compares the power-law fit from the zeroth and first iterations in this case.

Capillary 2 (dimensions 20 mm x 4 mm) – 0th Iteration						
Velocity	ΔP [MPa]	L [m]	v [m/s]	Q [m³/s]	τ_w [MPa]	$\dot{\gamma}_N$ [1/s]
1	0.29	0.105	0.00098	4.93×10^{-6}	0.0055	92.5
2	0.341	0.105	0.0028	1.39×10^{-5}	0.0065	260.8
3	0.484	0.105	0.0098	4.94×10^{-5}	0.0092	926.5
3	0.498	0.105	0.0099	4.96×10^{-5}	0.0095	929.7
4	0.497	0.105	0.010	5.03×10^{-5}	0.0095	944.2
5	0.474	0.105	0.016	7.92×10^{-5}	0.009	1485.9

Table 20: Results of the zeroth iteration for capillary 2 using the second approach

Capillary 2 (dimensions 20 mm x 4 mm) – 1st Iteration						
Velocity	ΔP [MPa]	L [m]	v [m/s]	Q [m³/s]	τ_w [MPa]	$\dot{\gamma}_{NN}$ [1/s]
1	0.29	0.105	0.00098	4.93×10^{-6}	0.0055	173.6
2	0.341	0.105	0.0028	1.39×10^{-5}	0.0065	489.3
3	0.484	0.105	0.0098	4.94×10^{-5}	0.0092	1738.2
3	0.498	0.105	0.0099	4.96×10^{-5}	0.0095	1744.3
4	0.497	0.105	0.010	5.03×10^{-5}	0.0095	1771.5
5	0.474	0.105	0.016	7.92×10^{-5}	0.009	2787.7

Table 21: Results of the first iteration for capillary 2 using the second approach

Capillary 2 Results			
Iteration Number	n [-]	K [Pa.s^{n}]	R^2
0	0.21	2146	0.9052
1	0.21	1882	0.9052

Table 22: Power-law results for capillary 2 using the second approach

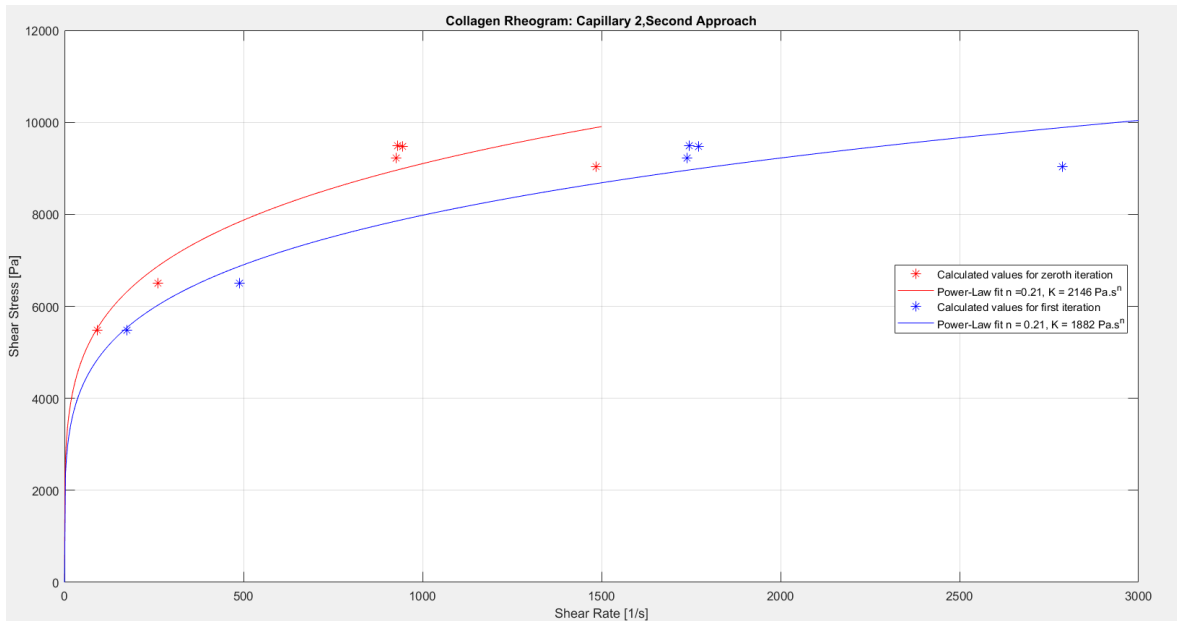


Figure 35: Comparison of the resulting rheograms for capillary 2 using the second approach

The results of capillary 3 using the second approach are shown in tables 23, 24, and 25. The rheogram of both iterations is shown in figure 36.

Capillary 3 (dimensions 20 mm x 2 mm) – 0th Iteration						
Velocity	ΔP [MPa]	L [m]	v [m/s]	Q [m³/s]	τ_w [MPa]	$\dot{\gamma}_N$ [1/s]
1	0.579	0.105	0.00089	4.47×10^{-6}	0.0055	335
2	0.755	0.105	0.0025	1.27×10^{-5}	0.0072	954.4
3	0.951	0.105	0.0053	2.66×10^{-5}	0.0091	1991.7
4	-	-	-	-	-	-
4	1.059	0.105	0.0095	4.75×10^{-5}	0.01	3564.5
5	1.152	0.105	0.016	8.24×10^{-5}	0.011	6181.9

Table 23: Results of the zeroth iteration for capillary 3 using the second approach

Capillary 3 (dimensions 20 mm x 2 mm) – 1st Iteration						
Velocity	ΔP [MPa]	L [m]	v [m/s]	Q [m³/s]	τ_w [MPa]	$\dot{\gamma}_{NN}$ [1/s]
1	0.579	0.105	0.00089	4.47×10^{-6}	0.0055	703.3
2	0.755	0.105	0.0025	1.27×10^{-5}	0.0072	2003.4
3	0.951	0.105	0.0053	2.66×10^{-5}	0.0091	4180.7
4	-	-	-	-	-	-
4	1.059	0.105	0.0095	4.75×10^{-5}	0.01	7482.4
5	1.152	0.105	0.016	8.24×10^{-5}	0.011	12976.6

Table 24: Results of the first iteration for capillary 3 using the second approach

Capillary 3 Results			
Iteration Number	n [-]	K [Pa.s^{n}]	R^2
0	0.23	1478	0.9833
1	0.23	1244	0.9833

Table 25: Power-law results for capillary 3 using the second approach

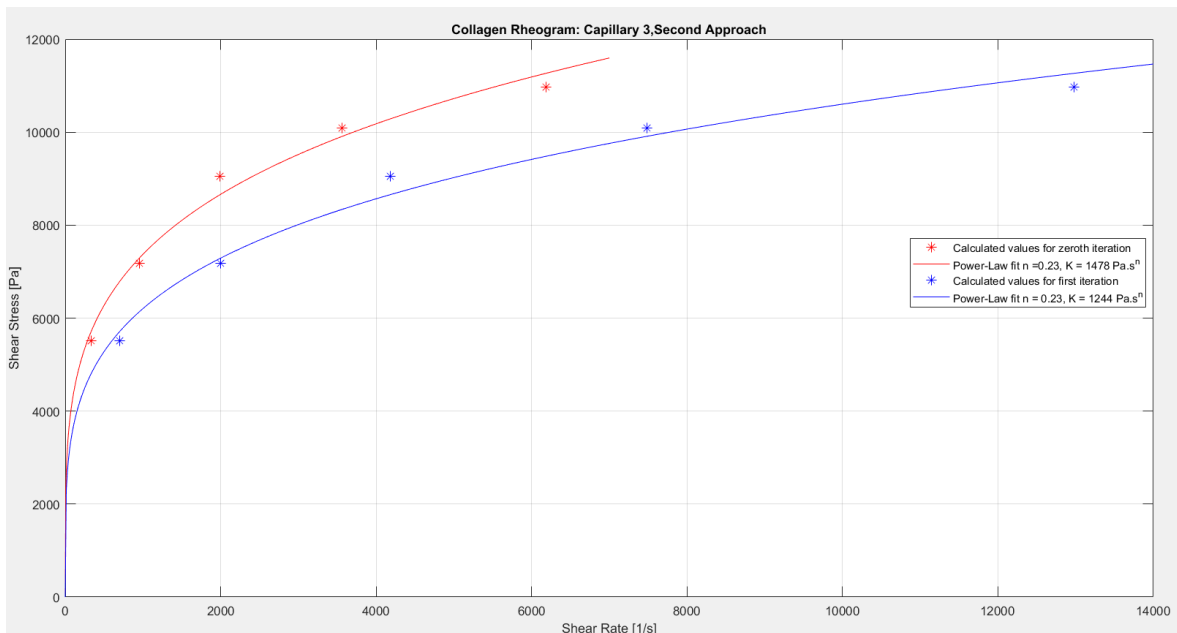


Figure 36: Comparison of the resulting rheograms for capillary 3 using the second approach

Tables 26, 27, and 28 show the results of re-extruded collagen using the second approach (parallel plates). Furthermore, figure 37 shows the power-law fit for both iterations.

Re-extruded Collagen Capillary 3 – 0th Iteration						
Velocity	ΔP [MPa]	L [m]	v [m/s]	Q [m³/s]	τ_w [MPa]	$\dot{\gamma}_N$ [1/s]
1	0.539	0.105	0.00083	4.16×10^{-6}	0.0051	311.6
3	0.895	0.105	0.0058	2.9×10^{-5}	0.0085	2172.04
5	1.071	0.105	0.013	6.77×10^{-5}	0.01	5079.6

Table 26: Results of the zeroth iteration for capillary 3 using the second approach and re-extruded collagen

Re-extruded Collagen Capillary 3 – 0th Iteration						
Velocity	ΔP [MPa]	L [m]	v [m/s]	Q [m³/s]	τ_w [MPa]	$\dot{\gamma}_{NN}$ [1/s]
1	0.539	0.105	0.00083	4.16×10^{-6}	0.0051	634.1
3	0.895	0.105	0.0058	2.9×10^{-5}	0.0085	4420.2
5	1.071	0.105	0.013	6.77×10^{-5}	0.01	10337.1

Table 27: Results of the first iteration for capillary 3 using the second approach and re-extruded collagen

Re-extruded Collagen Capillary 3 Results			
Iteration Number	n [-]	K [Pa.s^{n}]	R^2
0	0.24	1287	0.997
1	0.24	1082	0.997

Table 28: Power-law results for capillary 3 using the second approach and re-extruded collagen

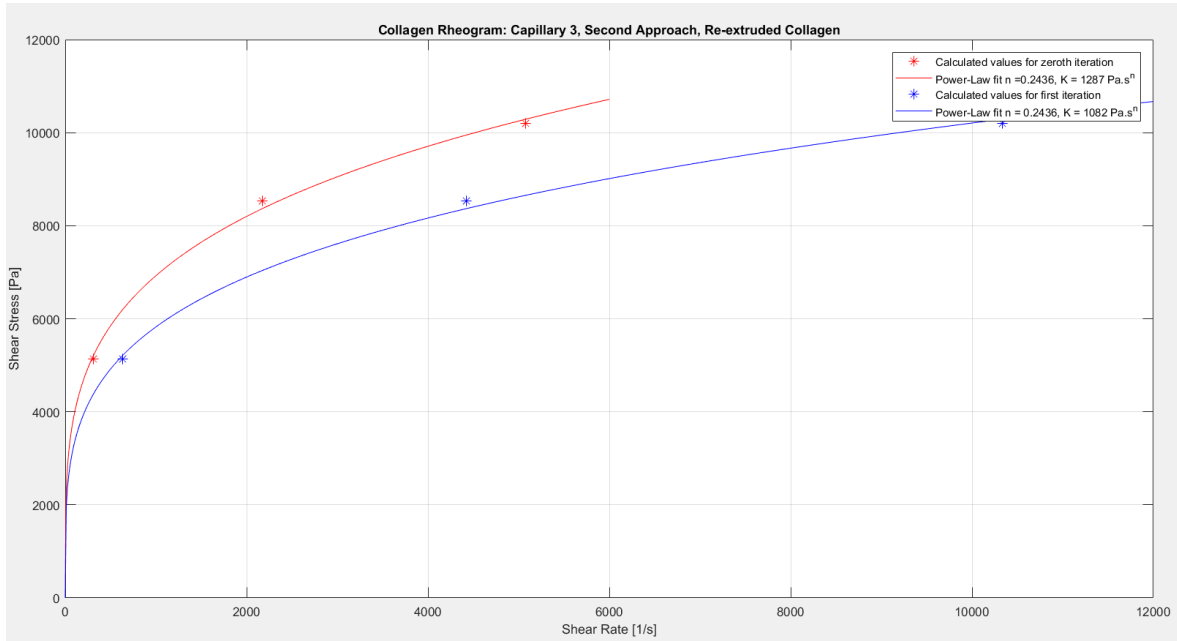


Figure 37: Comparison of the resulting rheograms for capillary 3 using the second approach and re-extruded collagen

Finally, the results of the third approach (rectangular slit) are presented below. In this case, the velocity of collagen is calculated as shown in the following tables of results. Tables 29 and 30 show the results of capillary 1 using the third approach. In this case, collagen velocity was is calculated rather than the shear rate. Figure 38 shows the resulting fit.

Capillary 1						
Velocity	ΔP [MPa]	L [m]	v [m/s]	Q [m³/s]	Collagen velocity [m/s]	τ_w [MPa]
1	0.133	0.105	0.00098	4.91×10^{-6}	0.031	0.0036
1	0.134	0.105	0.0010	5.05×10^{-6}	0.032	0.0037
1	0.142	0.105	0.0010	5.03×10^{-6}	0.031	0.0039
2	0.159	0.105	0.0023	1.18×10^{-5}	0.074	0.0043
3	0.208	0.105	0.0092	4.63×10^{-5}	0.29	0.0056
4	0.205	0.105	0.0087	4.38×10^{-5}	0.27	0.0056
5	0.221	0.105	0.017	8.61×10^{-5}	0.54	0.006

Table 29: Results for capillary 1 using the third approach

Capillary 1 Results		
n [-]	K [Pa.s^{n}]	R^2
0.19	1722	0.9905

Table 30: Power-law results for capillary 1 using the third approach

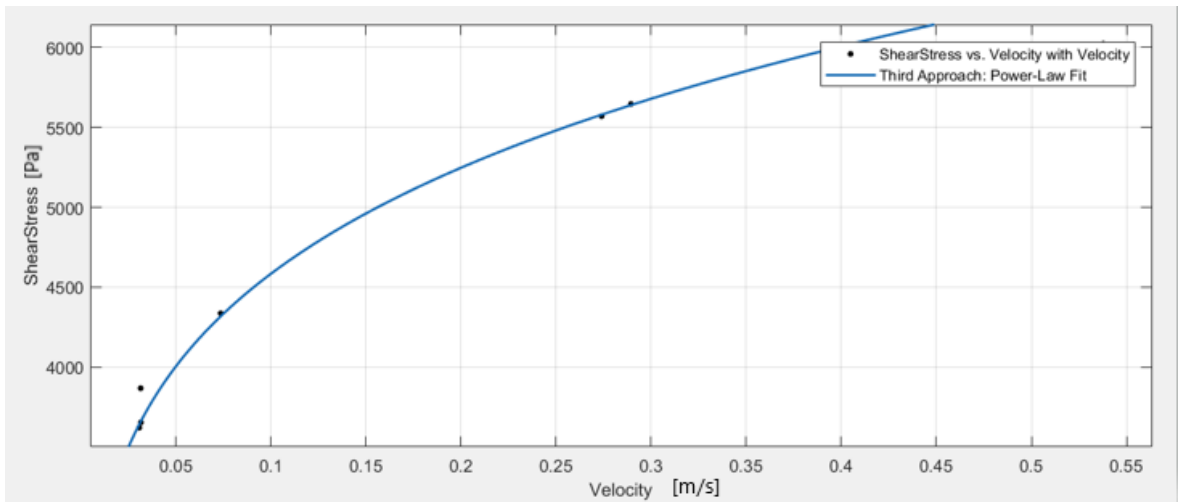


Figure 38: Resulting fit for capillary 1 using the third approach

The next tables outline the results of capillaries 2, 3, and re-extruded collagen using the third approach. Furthermore, the resulting fits are also shown following the tables of results for each capillary.

Capillary 2						
Velocity	ΔP [MPa]	L [m]	v [m/s]	Q [m ³ /s]	Collagen velocity [m/s]	τ_w [MPa]
1	0.29	0.105	0.00098	4.93x10 ⁻⁶	0.062	0.0046
2	0.341	0.105	0.0028	1.39x10 ⁻⁵	0.17	0.0054
3	0.484	0.105	0.0098	4.94x10 ⁻⁵	0.62	0.0077
3	0.498	0.105	0.0097	4.96x10 ⁻⁵	0.62	0.0079
4	0.497	0.105	0.010	5.03x10 ⁻⁵	0.63	0.0079
5	0.474	0.105	0.016	7.92x10 ⁻⁵	0.99	0.0075

Table 31: Results for capillary 2 using the third approach

Capillary 2 Results		
n [-]	K [Pa.s ⁿ]	R ²
0.21	1542	0.9052

Table 32: Power-law results for capillary 2 using the third approach

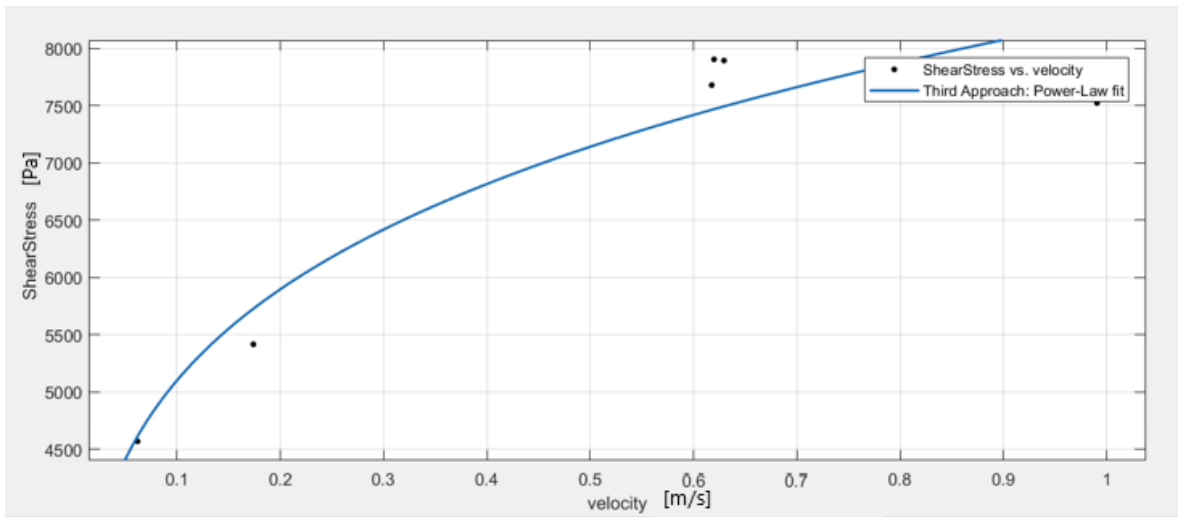


Figure 39: Resulting fit for capillary 2 using the third approach

Capillary 3						
Velocity	ΔP [MPa]	L [m]	v [m/s]	Q [m ³ /s]	Collagen velocity [m/s]	τ_w [MPa]
1	0.579	0.105	0.00089	4.47×10^{-6}	0.11	0.005
2	0.755	0.105	0.0025	1.27×10^{-5}	0.32	0.0065
3	0.951	0.105	0.0053	2.66×10^{-5}	0.66	0.0082
4	-	-	-	-	-	-
4	1.059	0.105	0.0095	4.75×10^{-5}	1.19	0.0092
5	1.152	0.105	0.016	8.24×10^{-5}	2.06	0.0099

Table 33: Results for capillary 3 using the third approach

Capillary 3 Results		
n [-]	K [Pa.s ⁿ]	R ²
0.23	1140	0.9833

Table 34: Power-law results for capillary 3 using the third approach

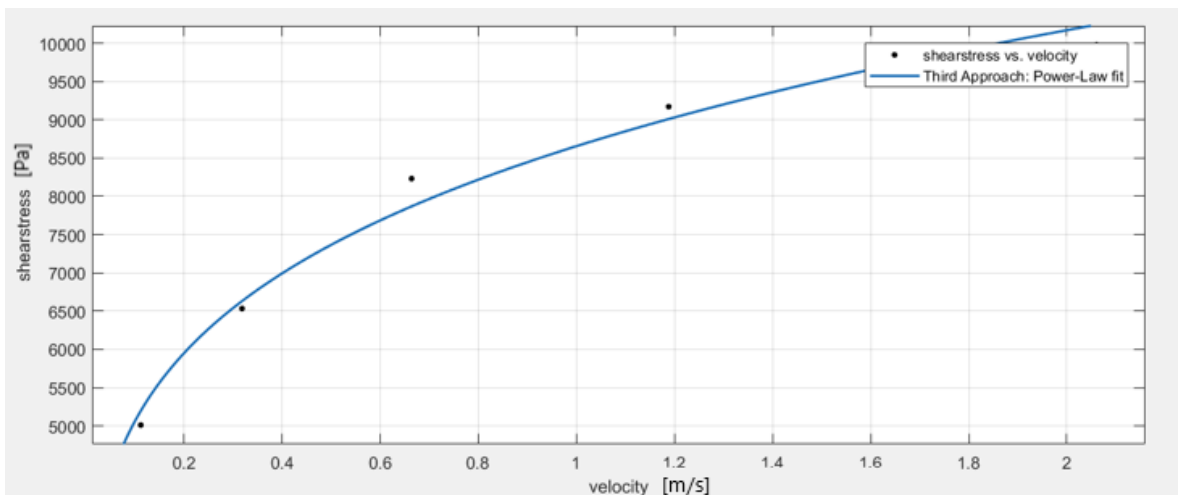


Figure 40: Resulting fit for capillary 3 using the third approach

Re-extruded Collagen Capillary 3						
Velocity	ΔP [MPa]	L [m]	v [m/s]	Q [m ³ /s]	Collagen velocity [m/s]	τ_w [MPa]
1	0.539	0.105	0.00083	4.16x10 ⁻⁶	0.10	0.0047
3	0.895	0.105	0.0058	2.9x10 ⁻⁵	0.72	0.0078
5	1.071	0.105	0.013	6.77x10 ⁻⁵	1.69	0.0093

Table 35: Results for capillary 3 using the third approach and re-extruded collagen

Re-extruded Collagen Capillary 3 Results		
n [-]	K [Pa.s ⁿ]	R ²
0.24	1091	0.997

Table 36: Power-law results for capillary 3 using the third approach and re-extruded

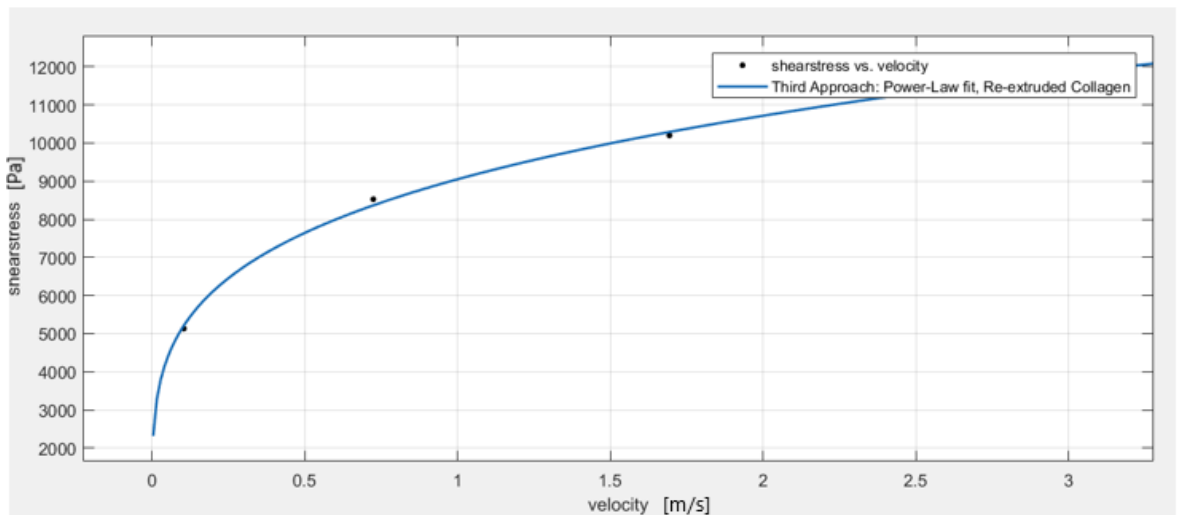


Figure 41: Resulting fit for capillary 3 using the third approach and re-extruded collagen

Table 37 outlines all the obtained results from each approach for each capillary. Evidently, the investigated collagen material exhibits a shear thinning (pseudoplastic) behaviour. Referring to the study done on acylated pepsin-solubilized collagen extracted from calf skin and modelled using the power-law, collagen was found to have a power law index of $n = 0.42$ [41]. A similar study by *J. Skočilas et al.* on collagen material with a mass fraction of 8 % found the power-law index to be $n = 0.25$. Furthermore, Ing. Jan Stipek, who performed the same experiments on collagen matter (dry-content of 7.8 %) found the power-law index for Capillaries 1, 2, and 3 to be an average of $n = 0.22$, $n = 0.21$ and, $n = 0.21$, respectively. On the other hand, Serdar Can Arslanturk, performed the same experiments on collagen (using the same capillary rheometer) with a dry content of 9.5 % found the power-law indices to be: $n = 0.3$ for capillary 1, $n = 0.18$ for capillary 2, and $n = 0.3$ for capillary 3. A key difference between the afore-mentioned studies and this work is in the method of data processing. Rather than plotting a rheogram from each experiment, a set of points of shear stresses and their corresponding shear rates evaluated from five velocities were used to create a single rheogram. The power-law model was then applied for each slit die. The resulting

parameters of the power law model were then used to recalculate the non-Newtonian shear rates depending on the used approach. Furthermore, the method of data processing is simplified by omitting the use of the Bagley correction. Using this method, the resulting power-law indices fall into the range described in *J. Skočilas et al.*

From table 37, for capillary 1, the power-law indices for the first and second approaches are equal. While for capillaries 2 and 3, the resulting power-law indices were the same for all approaches. Figures 42, 43 and 44 compare the rheograms of each capillary corresponding to the first and second approaches. Evidently, the second approach, denoted by the blue lines and markers, resulted in higher values of wall shear stress compared to the first approach. While having slightly lower flow indices, capillary 1 had the highest consistency coefficients.

	<i>Capillary 1</i>		<i>Capillary 2</i>		<i>Capillary 3</i>	
	<i>n [-]</i>	<i>K [Pa.sⁿ]</i>	<i>n [-]</i>	<i>K [Pa.sⁿ]</i>	<i>n [-]</i>	<i>K [Pa.sⁿ]</i>
<i>Approach 1</i>	0.18	1751	0.21	1374	0.23	918
<i>Approach 2</i>	0.18	2543	0.21	1882	0.23	1244
<i>Approach 3</i>	0.19	1722	0.21	1542	0.23	1140

Table 37: Summary of all results from the three approaches

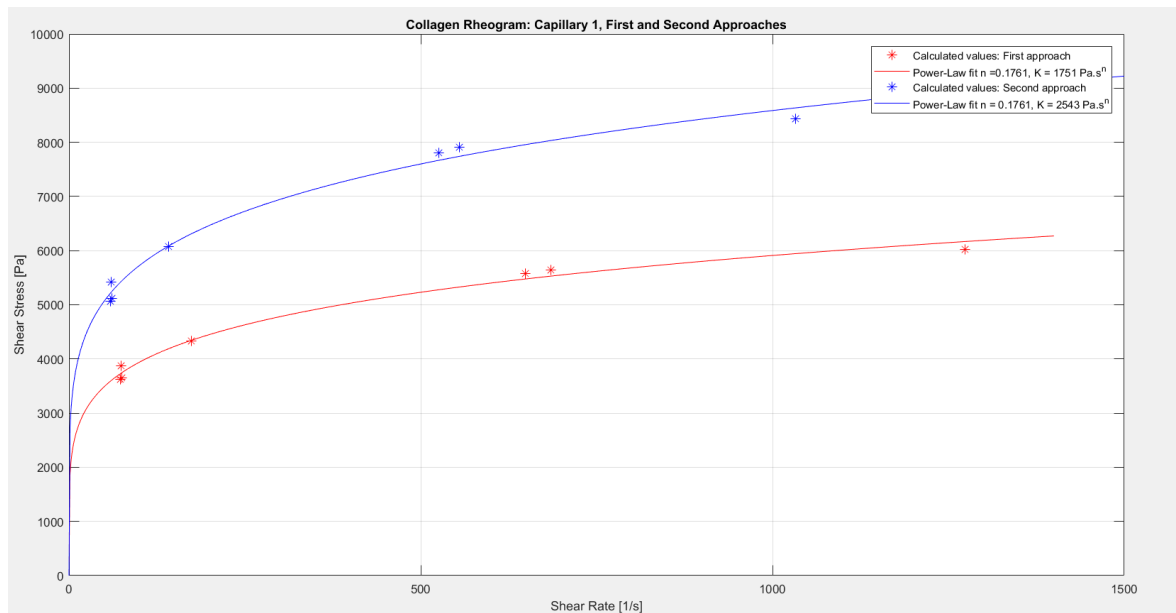


Figure 42: Comparison of the first and second approaches for capillary 1

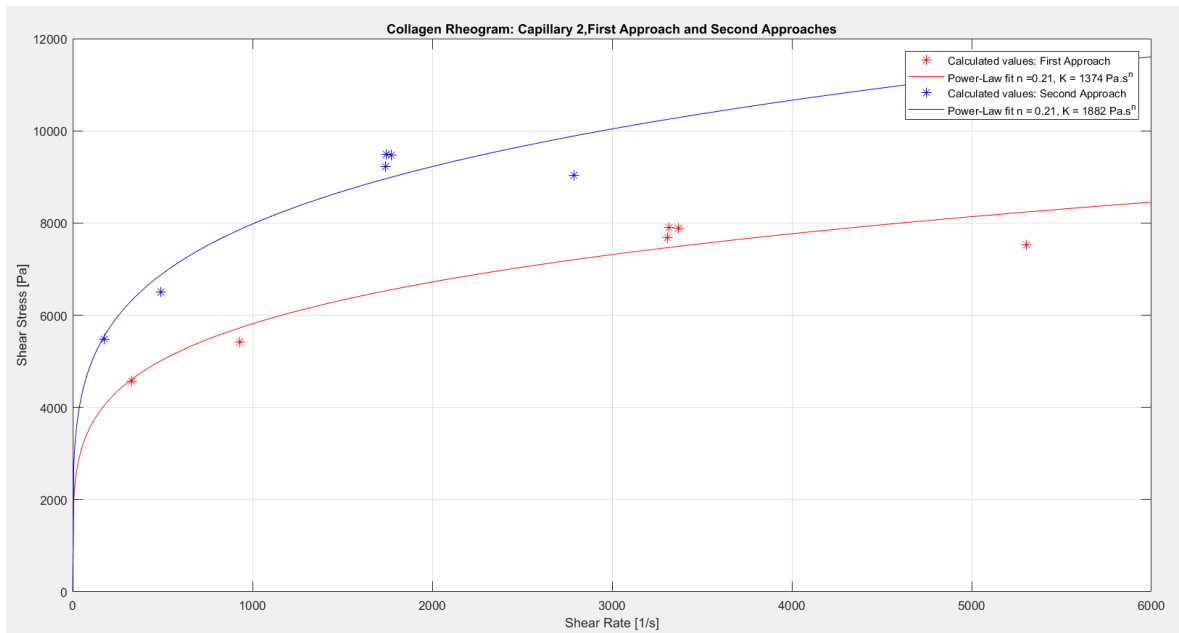


Figure 43: Comparison of the first and second approaches for capillary 2

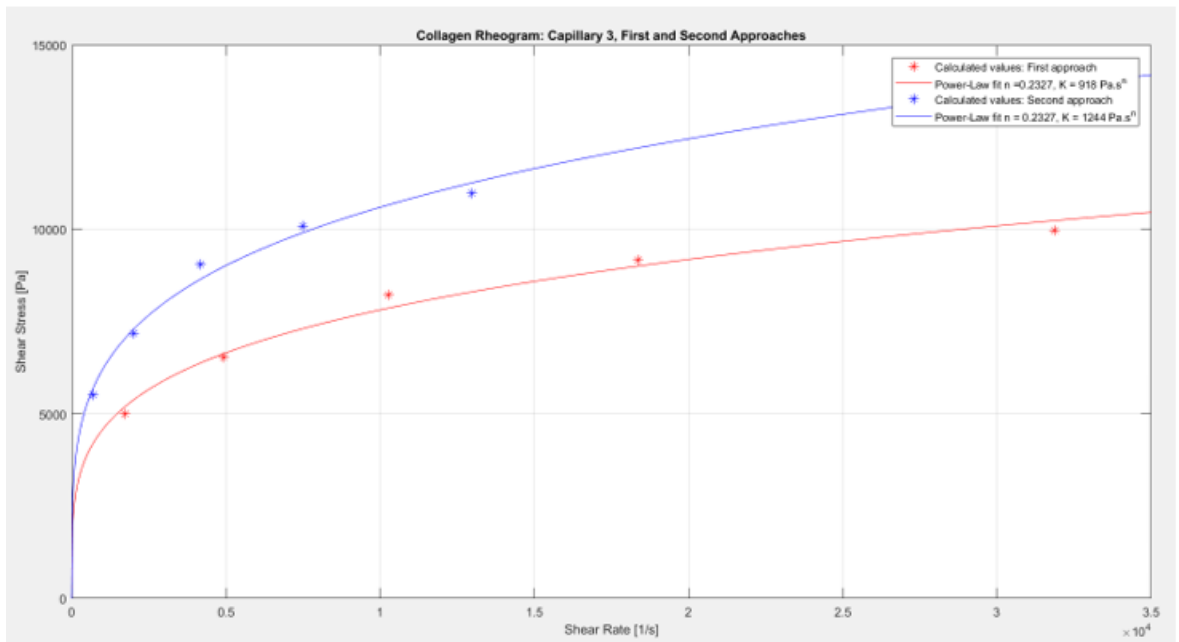


Figure 44: Comparison of the first and second approaches for capillary 3

Table 38 outlines the results for re-extruded collagen from the three approaches. The re-extrusion was done with capillary 3 and three different piston velocities. The results of the power-law index of re-extruded collagen fall approximately in the range of previously obtained results prior to re-extrusion, while displaying slightly lower consistency coefficients. Evidently, the re-extruded collagen had the same power-law indices for all three approaches. The temperature change in the re-extruded collagen was a negligible 1.5 °C. Figure 45 compares the rheograms corresponding to the first and second approaches for re-extruded collagen.

Re-extruded Collagen Capillary 3

	n [-]	K [Pa.s ⁿ]
Approach 1	0.24	790
Approach 2	0.24	1082
Approach 3	0.24	1091

Table 38: Summary of all results from the three approaches for re-extruded collagen

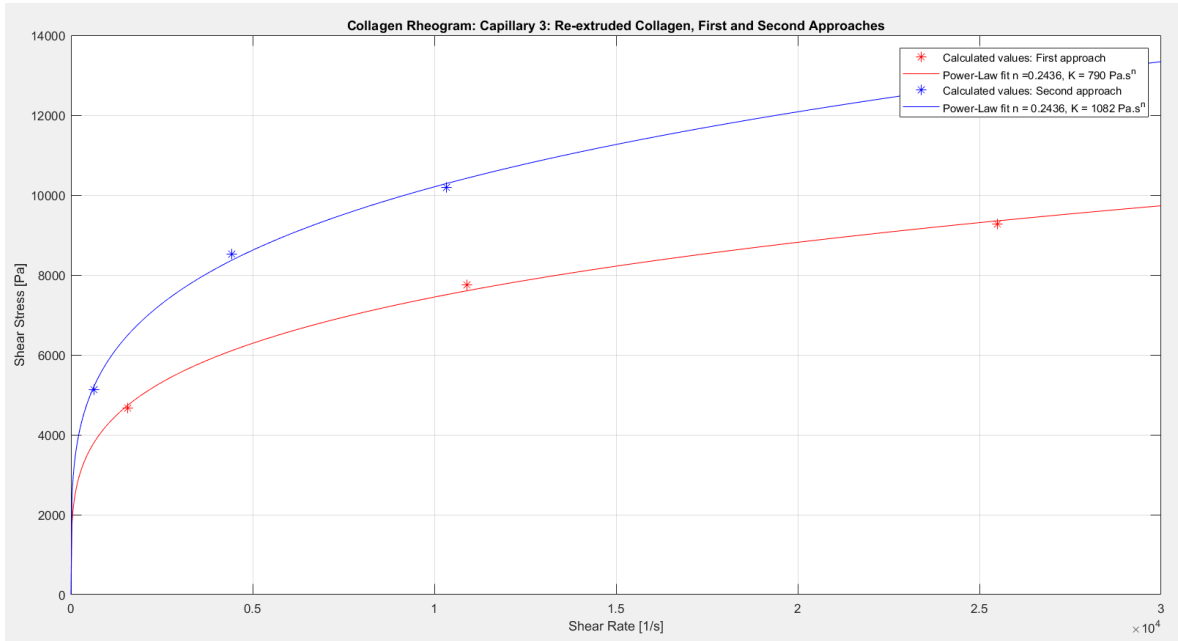


Figure 45: Comparison of the first and second approaches for capillary 3 and re-extruded collagen

To conclude the results, the shear stresses calculated by the third approach (rectangular slit) are plotted against the shear rates obtained from the second approach (parallel plates). In this way, the resulting flow index and consistency coefficient of collagen are found by combining the results of all capillaries that were used in the measurements. Figure 46 shows the final rheogram of the investigated collagen material.

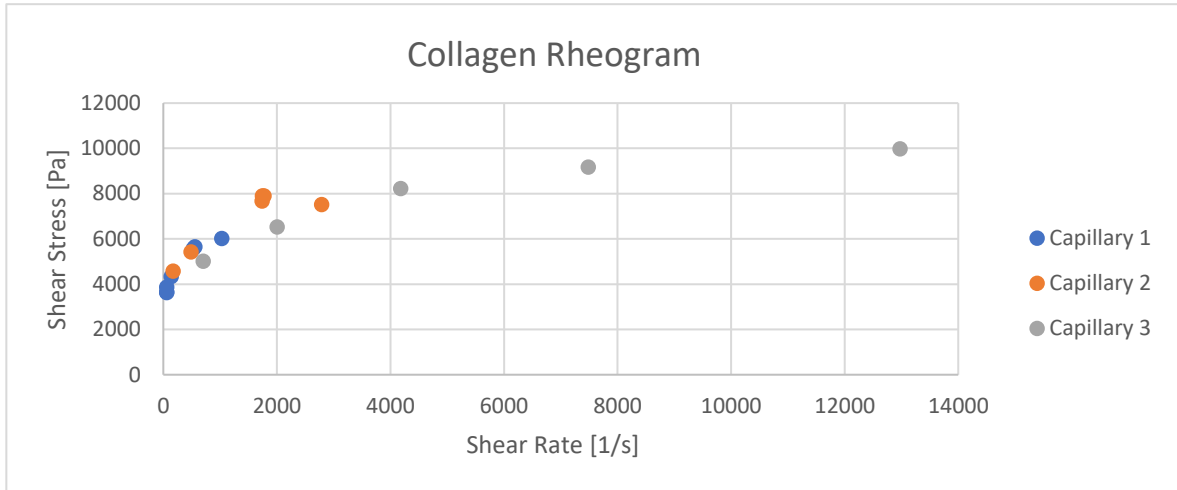


Figure 46: Collagen rheogram created from resulting data of all three capillaries

When the points presented in figure 46 are fit to a power-law model, the final parameters can be approximated. Figure 47 shows the power-law fit in a log-log plot of the shear stresses and shear strains.

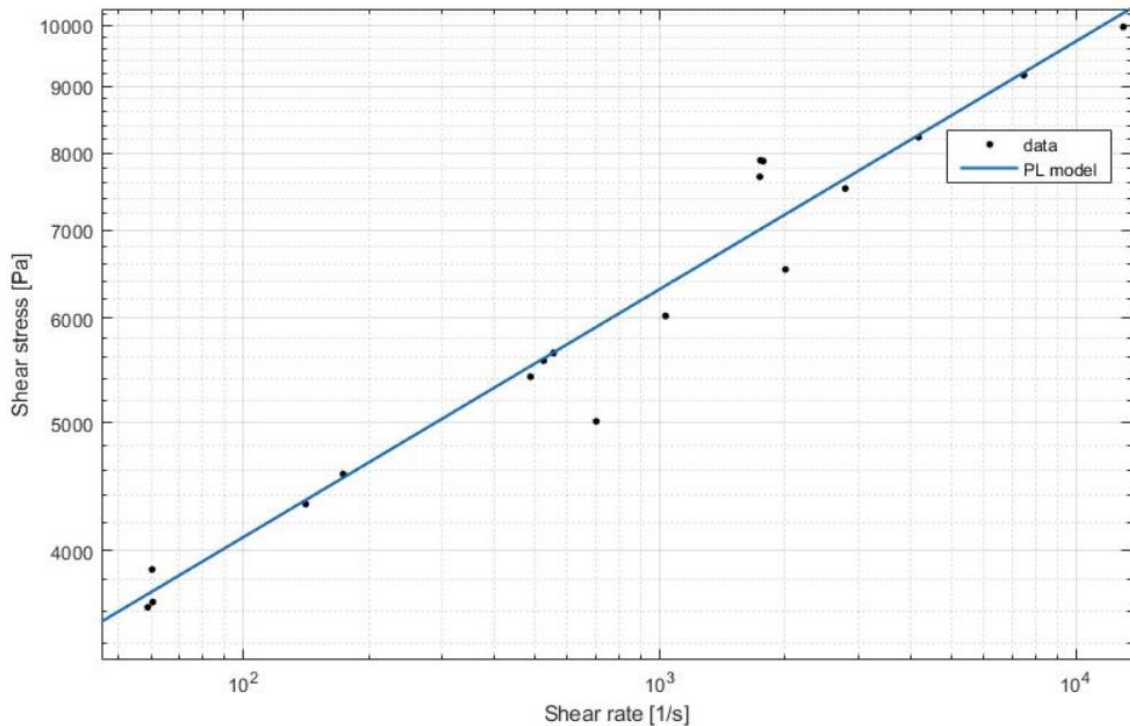


Figure 47: Results of the power-law model for collagen

From the regression analysis of all capillaries together, values of the parameters of the power law model, shown in table 39, were obtained with a confidence interval of 95 % for the investigated collagen material. It seems from the results that there is a deviation between parameters of the power-law model for different capillaries. However, the same results for different capillaries were expected. The deviations can be caused by the presence of air bubbles in collagen matter generated by the extrusion of matter with air cavities in the rheometer's cylindrical section. In addition, the deviations seen in the results may be also caused by the existence of noise in recorded data and the inability of the apparatus to maintain a constant piston velocity. Compared with historically published results, the obtained data are in good agreement. Experimental methodology must be improved, mainly by increasing the measuring points in the available shear rate range.

Three approaches were utilized to show the effect of the correction on results. It is obvious, according to the literature review, that the last approach involving all corrections should be the most valid for data evaluation.

n [-]	K [Pa.s^{n}]	R^2	SSE
0.19 ± 0.025	1721 ± 330	0.946	3.483x10 ⁶

Table 39: Results of the power-law model for collagen

4 Conclusion

The aim of this work was to identify the flow properties of native bovine-extracted collagen material by performing a literature search of collagen and flow in slit and capillary rheometers, acquainting with the experimental equipment in the laboratory, and assembling a MATLAB script for data evaluation. From the literature findings, an appropriate experimental method resembling several industrial applications of collagen processing was chosen. Furthermore, the power-law model was utilized given its versatility and simplicity as a two-parameter model. The experiments were done using a self-made capillary rheometer equipped with slit dies of different dimensions (2, 4 and 8 mm) all manufactured at the Czech Technical University in Prague.

By altering the equations for the flow through capillaries, MATLAB scripts were created in effect to model the behaviour of collagen. A unique way of data processing involving three approaches was applied in which several points of a rheogram are calculated first. Then, by utilizing the curve fitting tool with the least possible deviations, the data points are fit to a power-law model where a second iteration was applied. When the experimental recordings were evaluated in this manner, the flow index and consistency coefficient of collagen material were found and compared with prior studies and other approaches. Finally, the properties of re-extruded collagen were also assessed. Therefore, the aim of this thesis is fulfilled on the account of these findings.

The parameters of the power-law model of collagen matter are $n = 0.19$ and $K = 1721 \text{ Pa}\cdot\text{s}^n$ for collagen with a dry-content of 9.69 %. Hence, the obtained values are in good agreement with published data.

5 References

- [1] Douglas, M., Choi, J., & Clark, M. A. (2018). *Biology 2e*. Rice University. <https://openstax.org/books/biology-2e/pages/1-introduction> ISBN-13: 978-1-947172-53-1.
- [2] Mandal, D. A. (2019, June 5). *What is Collagen?* News. <https://www.news-medical.net/health/What-is-Collagen.aspx>.
- [3] Silvipriya, K., Kumar, K., Bhat, A., Kumar, B., John, A., & Lakshmanan, P. (2015). Collagen: Animal Sources and Biomedical Application. *Journal of Applied Pharmaceutical Science*, 123–127. <https://doi.org/10.7324/japs.2015.50322>
- [4] Frantz, C., Stewart, K. M., & Weaver, V. M. (2010). The extracellular matrix at a glance. *Journal of Cell Science*, 123(24), 4195–4200. <https://doi.org/10.1242/jcs.023820>
- [5] Fratzl, P. (2010). *Collagen: structure and mechanics*. Springer. e-ISBN: 978-0-387-73906-9
- [6] Gelse, K. (2003). Collagens—structure, function, and biosynthesis. *Advanced Drug Delivery Reviews*, 55(12), 1531–1546. <https://doi.org/10.1016/j.addr.2003.08.002>
- [7] Lin, K., Zhang, D., Macedo, M. H., Cui, W., Sarmiento, B., & Shen, G. (2018). Advanced Collagen-Based Biomaterials for Regenerative Biomedicine. *Advanced Functional Materials*, 29(3), 1804943. <https://doi.org/10.1002/adfm.201804943>
- [8] Schmidt, M.M. & Prestes Dornelles, Rosa & Mello, Renius & Kubota, E.H. & Mazutti, Marcio & Kempka, Aniela & Demiate, Ivo. (2016). Collagen extraction process. *International Food Research Journal* 23(3): 913-922 (2016). [http://www.ifrj.upm.edu.my/23%20\(03\)%202016/\(1\).pdf](http://www.ifrj.upm.edu.my/23%20(03)%202016/(1).pdf)
- [9] Soroushanova, A., Delgado, L. M., Wu, Z., Shologu, N., Kshirsagar, A., Raghunath, R., ... Zeugolis, D. I. (2018). The Collagen Suprafamily: From Biosynthesis to Advanced Biomaterial Development. *Advanced Materials*, 31(1), 1801651. <https://doi.org/10.1002/adma.201801651>
- [10] Kronick, P. L., & Cooke, P. (1996). Thermal Stabilization of Collagen Fibers by Calcification. *Connective Tissue Research*, 33(4), 275–282. <https://doi.org/10.3109/03008209609028885>
- [11] Wang, X., Bank, R. A., Tekoppele, J. M., & Agrawal, C. M. (2001). The role of collagen in determining bone mechanical properties. *Journal of Orthopaedic Research*, 19(6), 1021–1026. [https://doi.org/10.1016/s0736-0266\(01\)00047-x](https://doi.org/10.1016/s0736-0266(01)00047-x)
- [12] Barnes, H. A. (2000). *A handbook of elementary rheology*. University of Wales. Institute of Non-Newtonian Fluid Mechanics. ISBN 0-9538032-0-1
- [13] Doraiswamy, Deepak. (2002). The Origins of Rheology: A Short Historical Excursion. *Rheology Bulletin*. 71.

- [14] Walters, K. (2010). History of Rheology. In *Encyclopedia of Life Support Systems*. ISBN-978-1-84826-325-3.
- [15] Mezger, T. G., Sprinz, C., & Green, A. (2018). *Applied rheology: with Joe Flow on rheology road*. Anton Paar.
- [16] Steffe, J. F. (1996). *Rheological methods in food process engineering*. Freeman Press. ISBN 0-9632036-1-4
- [17] Çengel Yunus A., Cimbala, J. M., & Turner, R. H. (2012). *Fundamentals of thermal fluid sciences*. McGraw-Hill Higher Education.
- [18] Chhabra, R. P., & Richardson, J. F. (2011). *Non-Newtonian flow and applied rheology: engineering applications*. Butterworth-Heinemann. ISBN 978-0-7506-8532-0. <https://doi.org/10.1016/B978-0-7506-8532-0.X0001-7>
- [19] Collyer, A. A. (1973). Time independent fluids. *Physics Education*, 8(5), 333–338. <https://doi.org/10.1088/0031-9120/8/5/009>
- [20] Macosko, C. W. (1994). *Rheology: principles, measurements, and applications*. VCH Publishers. ISBN 1-56081-579-5.
- [21] Seguire, Edward. (1988). Casson plastic viscosity and yield value. What they are and what they mean to the confectioner. *The Manufacturing Confectioner*. 11. 57-63.
- [22] Sochi, T. (2010). Non-Newtonian flow in porous media. *Polymer*, 51(22), 5007–5023. <https://doi.org/10.1016/j.polymer.2010.07.047>
- [23] Moravec, F., & Letzelter, N. (2007). On the modeling of the linear viscoelastic behaviour of biological materials using Comsol Multiphysics. *Applied and Computational Mechanics*. ISSN 2336-1182
- [24] Binder, J. M., & Landig, A. J. (2009). The Kaye effect. *European Journal of Physics*, 30(6). <https://doi.org/10.1088/0143-0807/30/6/s03>
- [25] Han, C. D. (2007). *Rheology and processing of polymeric materials*. ProQuest Ebook Central. Oxford University Press. <https://ebookcentral.proquest.com/lib/cvut/reader.action?docID=415724>.
- [26] Friesenbichler, W., Neunhäuserer, A. & Duretek, I. Rheometry of polymer melts using processing machines. *Korea-Aust. Rheol. J.* 28, 167–174 (2016). <https://doi.org/10.1007/s13367-016-0016-5>
- [27] Ergun, R., Guo, J., & Huebner-Keese, B. (2016). Cellulose. *Encyclopedia of Food and Health*, 694–702. <https://doi.org/10.1016/b978-0-12-384947-2.00127-6>
- [28] Ghannam, M. T., & Esmail, M. N. (1997). Rheological properties of carboxymethyl cellulose. *Journal of Applied Polymer Science*, 64(2), 289–301. [https://doi.org/10.1002/\(sici\)1097-4628\(19970411\)64:23.0.co;2-n](https://doi.org/10.1002/(sici)1097-4628(19970411)64:23.0.co;2-n)

- [29] Benchabane, A., Bekkour, K. Rheological properties of carboxymethyl cellulose (CMC) solutions. *Colloid Polym Sci* 286, 1173 (2008). <https://doi.org/10.1007/s00396-008-1882-2>
- [30] Rabilloud, G. (2000). *High-performance polymers: chemistry and applications*. Éd. Technip.
- [31] McKeen, L. W. (2017). *Film properties of plastics and elastomers*. Elsevier. William Andrew. <https://www.elsevier.com/books/film-properties-of-plastics-and-elastomers/mckeen/978-0-12-813292-0>.
- [32] Jenekhe, S. A. (1983). The rheology and spin coating of polyimide solutions. *Polymer Engineering and Science*, 23(15), 830–834. <https://doi.org/10.1002/pen.760231508>
- [33] Jenekhe, S. A. (1983). Viscoelastic properties of polyamic acid solutions precursors of polyimides. *Polymer Engineering and Science*, 23(13), 713–718. <https://doi.org/10.1002/pen.760231305>
- [34] Chai, M., & Yeow, Y. (1990). Modelling of fluid M1 using multiple-relaxation-time constitutive equations. *Journal of Non-Newtonian Fluid Mechanics*, 35(2-3), 459–470. [https://doi.org/10.1016/0377-0257\(90\)85065-7](https://doi.org/10.1016/0377-0257(90)85065-7)
- [35] Sridhar, T. (1990). An overview of the project M1. *Journal of Non-Newtonian Fluid Mechanics*, 35(2-3), 85–92. [https://doi.org/10.1016/0377-0257\(90\)85039-2](https://doi.org/10.1016/0377-0257(90)85039-2)
- [36] Chellamuthu, M. (2010). *A comprehensive study of the extensional rheology of complex fluids* (dissertation). *A COMPREHENSIVE STUDY OF THE EXTENSIONAL RHEOLOGY OF COMPLEX FLUIDS*. Retrieved from https://scholarworks.umass.edu/cgi/viewcontent.cgi?referer=https://www.google.com/&httpsredir=1&article=1146&context=dissertations_1
- [37] Laun, H., & Hingmann, R. (1990). Rheological characterization of the fluid M1 and of its components. *Journal of Non-Newtonian Fluid Mechanics*, 35(2-3), 137–157. [https://doi.org/10.1016/0377-0257\(90\)85043-x](https://doi.org/10.1016/0377-0257(90)85043-x)
- [38] Skočilas, J., Žitný, R., Štancl, J., Dostál, M., Landfeld, A., & Houška, M. (2016). Rheological Properties of Collagen Matter Predicted Using an Extrusion Rheometer. *Journal of Texture Studies*, 47(6), 514–522. <https://doi.org/10.1111/jtxs.12194>
- [39] Skočilas, J., Žitný, R., Štancl, J., Solnař, S., Landfeld, A., & Houška, M. (2017). Flow of bovine collagen in rectangular slit. <https://doi.org/10.1063/1.4982995>
- [40] Tenchurin, T. K., Belousov, S. I., Kiryukhin, Y. I., Istranov, L. P., Istranova, E. V., Shepelev, A. D., ... Chvalun, S. N. (2018). Control on rheological behavior of collagen 1 dispersions for efficient electrospinning. *Journal of Biomedical Materials Research Part A*, 107(2), 312–318. <https://doi.org/10.1002/jbm.a.36459>
- [41] Li, C., Duan, L., Tian, Z., Liu, W., Li, G., & Huang, X. (2015). Rheological behavior of acylated pepsin-solubilized collagen solutions: Effects of concentration. *Korea-Australia Rheology Journal*, 27(4), 287–295. <https://doi.org/10.1007/s13367-015-0028-6>

6 Appendices

List of Symbols

A	[m ²]	Shear area
a, b	[-]	Geometric parameters
B, w	[m]	Capillary width
c	[Pa. s]	Flow coefficient; also called Herschel-Bulkley viscosity
D	[m]	Capillary tube diameter
D_h	[m]	Hydraulic diameter
F	[N]	Shear force
G	[Pa]	Shear modulus
H, h	[m]	Capillary height
h	[m]	Shear gap
K	[Pa. s ⁿ]	Consistency coefficient
K	[s]	Cross time constant (Consistency)
L	[m]	Capillary Tube length (or slit length)
m	[-]	Cross rate constant
n	[-]	Flow behaviour index or power-law index
p	[-]	Herschel-Bulkley index
P	[Pa]	Pressure
Q	[m ³ /s]	Volumetric flow rate
R	[m]	Radius of circular tube
V	[m/s]	Velocity
V	[m/s]	Mean velocity in capillary
v	[m/s]	Piston velocity

α -chains		Polypeptide chains of amino acids
$\dot{\gamma}$	[s ⁻¹]	Shear rate at shear flow
$\dot{\gamma}_N$	[1/s]	Shear rate for a Newtonian fluid at shear flow
$\dot{\gamma}_{NN}$	[1/s]	Shear rate for a non-Newtonian fluid at shear flow
ΔP	[Pa]	Pressure drop
η	[Pa. s]	Shear viscosity
η_∞	[Pa. s]	Infinite-shear viscosity
η_0	[Pa. s]	Zero-shear viscosity
η_B	[Pa. s]	Bingham plastic viscosity
η_C	[Pa. s]	Casson plastic viscosity
ν	[m ² /s]	Kinematic viscosity
ρ	[kg/m ³]	Density
σ_B	[Pa]	Bingham yield stress
σ_C	[Pa]	Casson yield stress
σ_{HB}	[Pa]	Herschel-Bulkley yield stress
τ	[Pa]	Shear stress
τ_w	[Pa]	Wall shear stress
CMC		Carboxymethyl cellulose
ECM		Extracellular Matrix
GNF		Generalized Newtonian Fluids
M1		Model fluid (constant viscosity elastic liquid)
PAA		Polyamic acid

List of Tables

Table 1: Capillary dimensions	41
Table 2: Number of experiments performed using each capillary and the corresponding velocity.....	44
Table 3: Recalculated radius for the flow through a slit.....	47
Table 4: Values of a and b recalculated for capillaries 1, 2, and 3	50
Table 5: Results of the zeroth iteration for capillary 1 using the first approach.....	51
Table 6: Results of the first iteration for capillary 1 using the first approach	51
Table 7: Power-law results for capillary 1 using the first approach	52
Table 8: Results of the zeroth iteration for capillary 2 using the first approach.....	52
Table 9: Results of the first iteration for capillary 2 using the first approach	52
Table 10: Power-law results for capillary 2 using the first approach	53
Table 11: Results of the zeroth iteration for capillary 3 using the first approach.....	53
Table 12: Results of the first iteration for capillary 3 using the first approach	53
Table 13: Power-law results for capillary 3 using the first approach	54
Table 14: Results of the zeroth iteration for capillary 3 using the first approach and re-extruded collagen.....	54
Table 15: Results of the first iteration for capillary 3 using the first approach and re-extruded collagen.....	54
Table 16: Power-law results for capillary 3 using the first approach and re-extruded collagen	54
Table 17: Results of the zeroth iteration for capillary 1 using the second approach	55
Table 18: Results of the first iteration for capillary 1 using the second approach	55
Table 19: Power-law results for capillary 1 using the second approach	56
Table 20: Results of the zeroth iteration for capillary 2 using the second approach.....	56
Table 21: Results of the first iteration for capillary 2 using the second approach	56
Table 22: Power-law results for capillary 2 using the second approach	57
Table 23: Results of the zeroth iteration for capillary 3 using the second approach	57
Table 24: Results of the first iteration for capillary 3 using the second approach	57
Table 25: Power-law results for capillary 3 using the second approach	58
Table 26: Results of the zeroth iteration for capillary 3 using the second approach and re-extruded collagen.....	58
Table 27: Results of the first iteration for capillary 3 using the second approach and re-extruded collagen.....	58

Table 28: Power-law results for capillary 3 using the second approach and re-extruded collagen.....	59
Table 29: Results for capillary 1 using the third approach.....	59
Table 30: Power-law results for capillary 1 using the third approach.....	59
Table 31: Results for capillary 2 using the third approach.....	60
Table 32: Power-law results for capillary 2 using the third approach.....	60
Table 33: Results for capillary 3 using the third approach.....	61
Table 34: Power-law results for capillary 3 using the third approach.....	61
Table 35: Results for capillary 3 using the third approach and re-extruded collagen.....	62
Table 36: Power-law results for capillary 3 using the third approach and re-extruded.....	62
Table 37: Summary of all results from the three approaches.....	63
Table 38: Summary of all results from the three approaches for re-extruded collagen.....	65
Table 39: Results of the power-law model for collagen.....	67

List of Figures

Figure 1: Structure of fibrillar collagen [7]	10
Figure 2: Individual layers of fluids in shear flow [15].....	15
Figure 3: Rheogram of typical Newtonian fluids [16].....	17
Figure 4: Viscosity curves for Silicon oils of different molecular weight [12].....	18
Figure 5: Flow curves of a shear-thinning fluid [15].....	20
Figure 6: Typical values of power-law constants [18]	21
Figure 7: Log-log plot of shear stress vs. shear rate of shear thickening and shear thinning fluids [19].....	24
Figure 8: Flow curves of time-independent fluids [18]	26
Figure 9: Time-dependent vs. time-independent flow behaviour [22]	27
Figure 10: Scheme of the Maxwell model [16]	29
Figure 11: Scheme of the Kelvin-Voigt model [16].....	29
Figure 12: Scheme of the Burgers model [16].....	30
Figure 13: The Kaye effect captured in a series of images [24]	31
Figure 14: Effects of viscoelasticity in viscous versus viscoelastic fluids [16].....	32
Figure 15: Rotational and tube type rheometers [16]	33
Figure 16: Plunger-type capillary rheometer [25]	34
Figure 17: Continuous-flow capillary rheometer [25].....	34
Figure 18: Slit rheometer [16]	35
Figure 19: Scheme of the capillary rheometer apparatus where $A=25$ mm, $B= 35$ mm and $D=80$ mm [39].....	40
Figure 20: Collagen sample	41
Figure 21: Capillary rheometer used for experimental measurements	42
Figure 22: Slit dies used in the extrusion capillary rheometer	42
Figure 23: Collagen extrusion through capillary slit rheometer	44
Figure 24: Example of acquired data after one measurement	45
Figure 25: Pressure profiles of the first experiment with capillary 1	45
Figure 26: Bold lines specify the approximate range from which the average pressure drop is calculated, capillary 1.....	46
Figure 27: Position of the piston vs. time	47
Figure 28: Piston velocity determined by linear regression	48
Figure 29: Typical values of a and b [18].....	50
Figure 30: Comparison of the resulting rheograms for capillary 1 using the first approach	52

Figure 31: Comparison of the resulting rheograms for capillary 2 using the first approach	53
Figure 32: Comparison of the resulting rheograms for capillary 3 using the first approach	54
Figure 33: Comparison of the resulting rheograms for capillary 3 using the first approach and re-extruded collagen.....	55
Figure 34: Comparison of the resulting rheograms for capillary 1 using the second approach	56
Figure 35: Comparison of the resulting rheograms for capillary 2 using the second approach	57
Figure 36: Comparison of the resulting rheograms for capillary 3 using the second approach	58
Figure 37: Comparison of the resulting rheograms for capillary 3 using the second approach and re-extruded collagen.....	59
Figure 38: Resulting fit for capillary 1 using the third approach.....	60
Figure 39: Resulting fit for capillary 2 using the third approach.....	61
Figure 40: Resulting fit for capillary 3 using the third approach.....	61
Figure 41: Resulting fit for capillary 3 using the third approach and re-extruded collagen	62
Figure 42: Comparison of the first and second approaches for capillary 1	63
Figure 43: Comparison of the first and second approaches for capillary 2	64
Figure 44: Comparison of the first and second approaches for capillary 3	64
Figure 45: Comparison of the first and second approaches for capillary 3 and re-extruded collagen.....	65
Figure 46: Collagen rheogram created from resulting data of all three capillaries	66
Figure 47: Results of the power-law model for collagen.....	66

Appendix A: Procedure of Calculation of a Point in Rheogram

The calculation of a point in the collagen rheogram for the three approaches is shown in the following. The calculation of piston velocity, collagen's volumetric flow rate and the mean pressure drop is common to all approaches. This example shows the calculation of from the data of capillary 3 (dimensions 20 mm x 2 mm). Beginning with the piston velocity, the data file '2mm_vell_exp1' is loaded to MATLAB. The duration of the experiment is found from the difference between the first and last absolute time points. The piston position is plotted against time which, in this case, is from 0 to 117.8 seconds. Figure I shows the piston position plotted against time. Evidently, to find the velocity, the slope of the constant velocity segment is calculated. Figure II shows the calculated velocity using Excel.

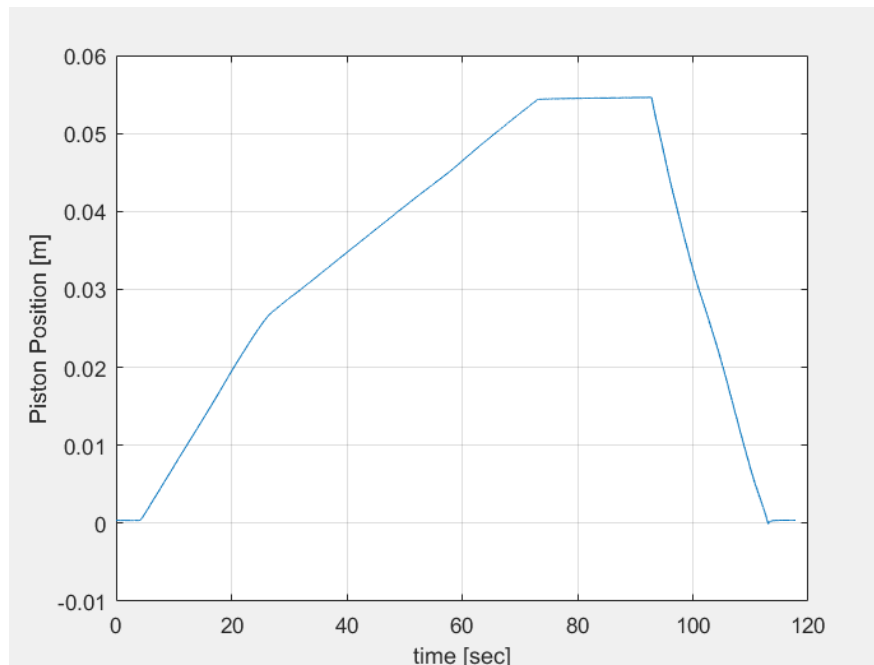


Figure I: Piston position vs. time

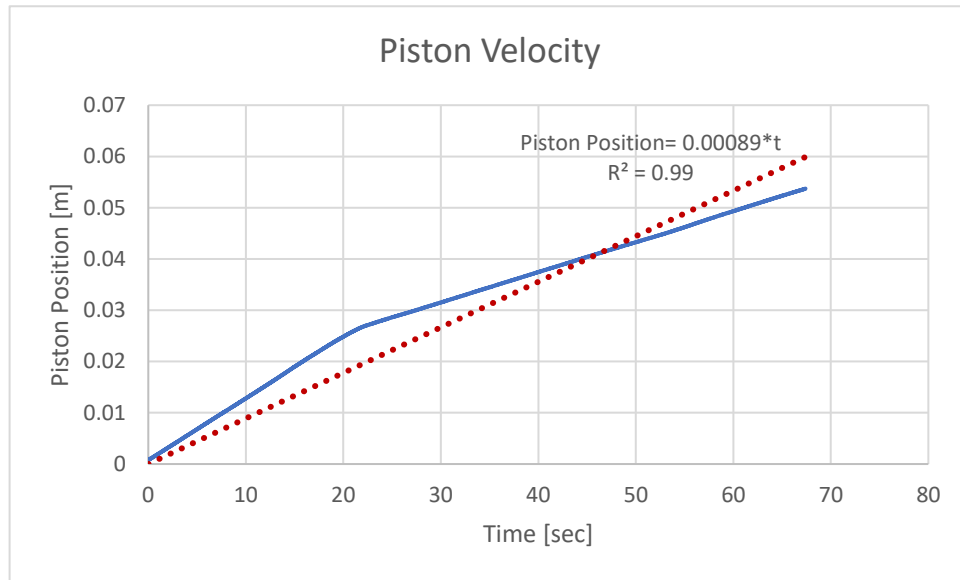


Figure II: Calculated piston velocity

Next, the volumetric flow rate of collagen is calculated using the following equation. The diameter of the capillary is 80 mm.

$$Q = A \cdot V$$

where:

Q [m^3/s] is volumetric flow rate

A [m^2] is capillary cross-sectional area

$$A = \pi \cdot R^2 = \pi \cdot (0.04)^2 = 0.00503 \text{ m}^2$$

$$Q = A \cdot V = 0.00503 \cdot 0.00089 = 4.467 \cdot 10^{-6} \frac{m^3}{s}$$

Then, the graph of pressure plotted against experimental time must be examined because measurements done with higher velocities have shorter durations. This means that the point at which the pressure drop is calculated from is subject to the velocity and duration of each experiment.

From this, the graph of pressures P1 to P6 (converted from bars to megapascals) can be plotted against time. Furthermore, the signals from P6 (inside the cylindrical container of rheometer) and P1 will be omitted for automatization of the data processing by script since some of the experimental data exhibited negative P1 values, which means that the capillary die was not filled. Then, by examining the pressure profiles, shown in figure III, the average value of the pressure drop is calculated using MATLAB.

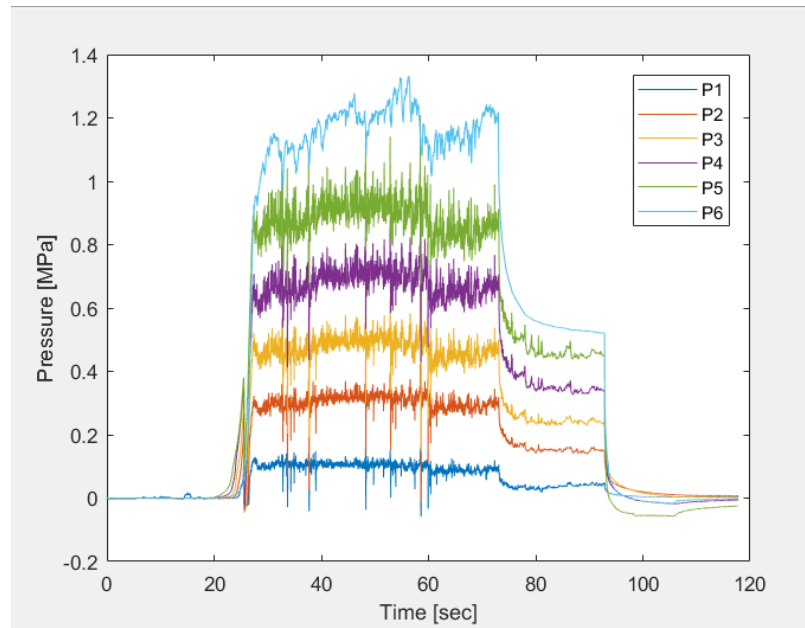


Figure III: Pressures P1 through P6 plotted against time

In this case, the pressure drop is calculated from the difference between the mean values of P5 and P2 in the interval 27 to 73 seconds.

$$\Delta P = \text{avg}(P5) - \text{avg}(P2) = 0.882414419 - 0.30363555 = 0.57877887 \text{ MPa}$$

$$\Delta P = 0.579 \text{ MPa}$$

In view of the calculated values, the three approaches can now be applied to find the power-law parameters using each approach.

- First Approach (hydraulic diameter):

As previously stated, the first approach is based on transforming the flow through a slit to flow through a straight circular pipe by employing the hydraulic diameter. In the case of capillary 3, the hydraulic diameter $D_h = 0.00363$ m. Then, the wall shear stress is calculated from the following formula, where the length L is the distance between pressure transducer P2 and P5 (L = 105 mm)

$$\tau_w = \frac{\Delta P \cdot R}{2L}$$

where:

τ_w [Pa] is wall shear stress

ΔP [Pa] is pressure drop

R [m] is radius of circular tube

$$R = \frac{D_h}{2} = \frac{0.00363}{2} = 0.00182 \text{ m}$$

$$\tau_w = \frac{0.57877887 \cdot 0.001818}{2 \cdot 0.105} = 0.00501 \text{ MPa}$$

Next, the Newtonian shear stress is calculated from the following formula:

$$\dot{\gamma}_N = \frac{4 \cdot Q}{\pi R^3} = \frac{4 \cdot 4.467 \cdot 10^{-6}}{\pi(0.001818)^3} = 946.3 \frac{1}{s}$$

The same procedure of calculation is then done on the remaining data files for a given capillary. The wall shear stresses are plotted against shear strains resulting in a rheogram which can then be fitted to the power-law model. In this case, the resulting power-law index for capillary 3, approach 1 is $n = 0.23$. These calculations are part of the ‘zeroth’ iteration. To begin the ‘first’ iteration, the resulting power-law index is used to calculate the non-Newtonian shear rate for a power-law fluid as shown in the following equation:

$$\dot{\gamma}_{NN} = \frac{Q}{\pi R^3} \left[3 + \frac{1}{n} \right]$$

$$\dot{\gamma}_{NN} = \frac{4.467 \cdot 10^{-6}}{\pi(0.001818)^3} \left[3 + \frac{1}{0.2327} \right] = 1726.32 \frac{1}{s}$$

Similarly, the same procedure of calculation is done for the remaining experiments where, once again, the power-law parameters are found.

- Second Approach (parallel plates):

The second approach is based on transforming the flow through a slit to flow in a very wide slot [15]. The wall shear-stresses are first calculated using the calculated pressure drop $\Delta P = 0.57877887 \text{ MPa}$ (same experiment using the same capillary). Hence, the calculations of wall shear stress in case of the flow through a very wide slot are done as follows:

$$\tau_w = \frac{\Delta P \cdot H}{2L} = \frac{0.5788 \cdot 0.002}{2(0.105)} = 0.00551 \text{ MPa}$$

and,

$$\dot{\gamma}_N = \frac{6 \cdot Q}{B \cdot H^2} = \frac{6 \cdot 4.467 \cdot 10^{-6}}{(0.02)(0.002)^2} = 335.02 \frac{1}{s}$$

Like the first approach, the remaining points are calculated in the same manner and fit to the power model. The resulting flow index in this case is $n = 0.2327$. Finally, the shear rate for a power-law fluid can be calculated as shown in the following:

$$\dot{\gamma}_{NN} = \frac{2 \cdot Q}{B \cdot H^2} \left[2 + \frac{1}{n} \right] = \frac{2 \cdot 4.467 \cdot 10^{-6}}{0.02(0.002)^2} \left[2 + \frac{1}{0.2327} \right] =$$

$$\dot{\gamma}_{NN} = 703.26 \frac{1}{s}$$

Once again, the same procedure of calculation is done for the remaining experiments where, the power-law parameters are found.

- Third Approach (rectangular slit):

The third approach is based on fitting the calculated wall shear stresses and collagen velocity to a power-law expression as shown below. First, the wall shear stresses are calculated using the same formula used in approach 1. Then, the velocity of collagen material is calculated by dividing the volumetric flow rate of collagen by the area of the slit. Then, the resulting wall shear-stresses are fit to the following equation by utilizing MATLAB's data fitting tool to a custom equation.

$$\tau_w = K \left(\frac{8 \cdot V}{D_h} \left(b + \frac{a}{n} \right) \right)^n$$

Parameters a and b are dimensionless geometrical parameters characterising the cross-section of the rectangular duct (slit). These parameters are obtained by interpolation from typical values listed in reference [18].